Wireless Communications

Lecture 4 - Radio wave propagation model in Small-scale Fading and Multipath

Small-scale Multipath Propagation

- Multipath in radio channel creates small-scale fading effects.
- The most important effects are:
  - Rapid changes in signal strength.
  - Random frequency modulation due to Doppler shifts.
  - Time dispersion (echoes) caused by multipath propagation delays.

Small-scale Fading

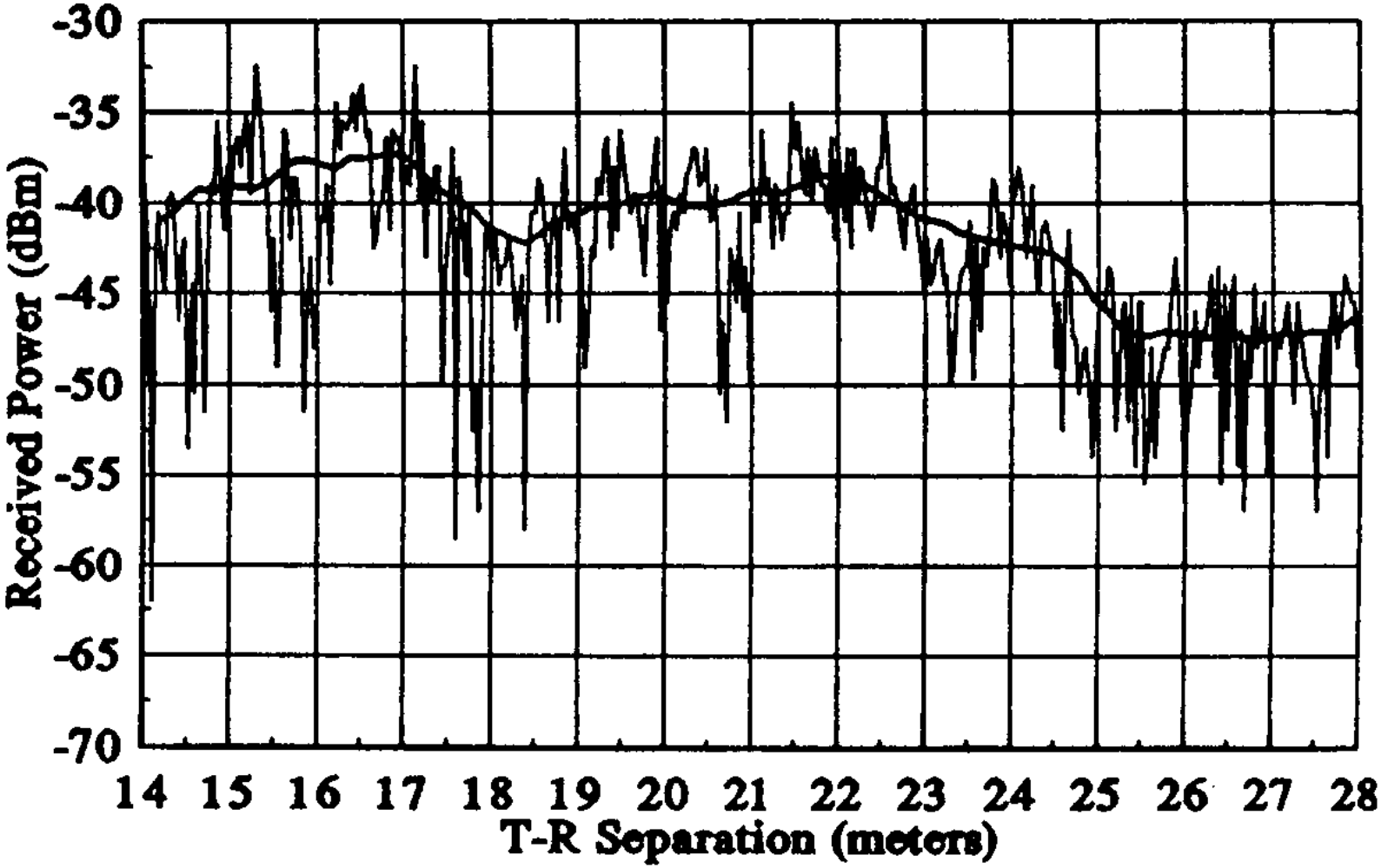

Doppler Shift Geometry

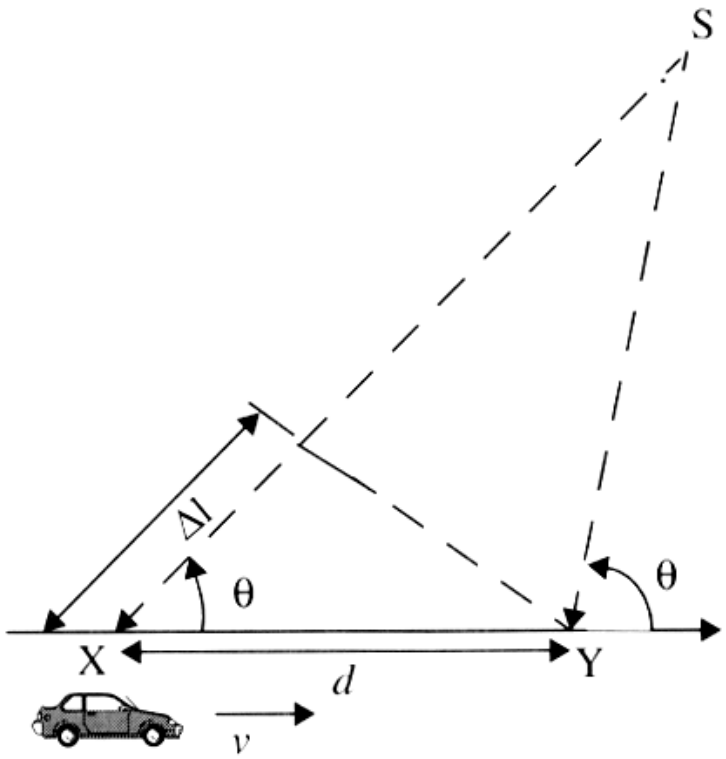

Figure 5.1 Illustration of Doppler effect.

Doppler Shift

- For an arbitrary ΔI value we have

$$\Delta\Phi = 2\pi\Delta I/\lambda.$$

- From Figure 5.1 we have $\Delta I = d \cdot \cos\theta$.
- Therefore the phase change becomes:

$$\Delta\Phi = 2\pi v \Delta t \cos\theta / \lambda.$$

- The Doppler frequency can be defined as the phase change due to the movement of the MS during the infinitesimal interval Δt:

$$f_d = v \cos\theta / \lambda.$$

Channel issues

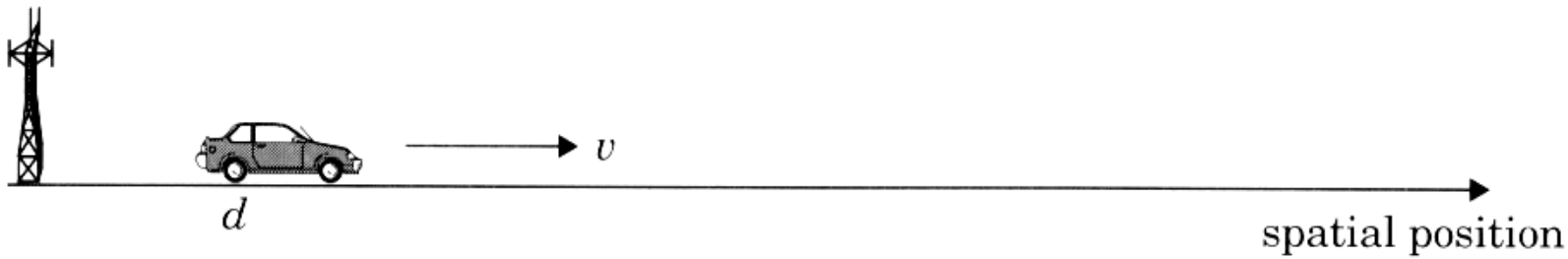

Figure 5.2 The mobile radio channel as a function of time and space.

Complex Baseband model for RF systems

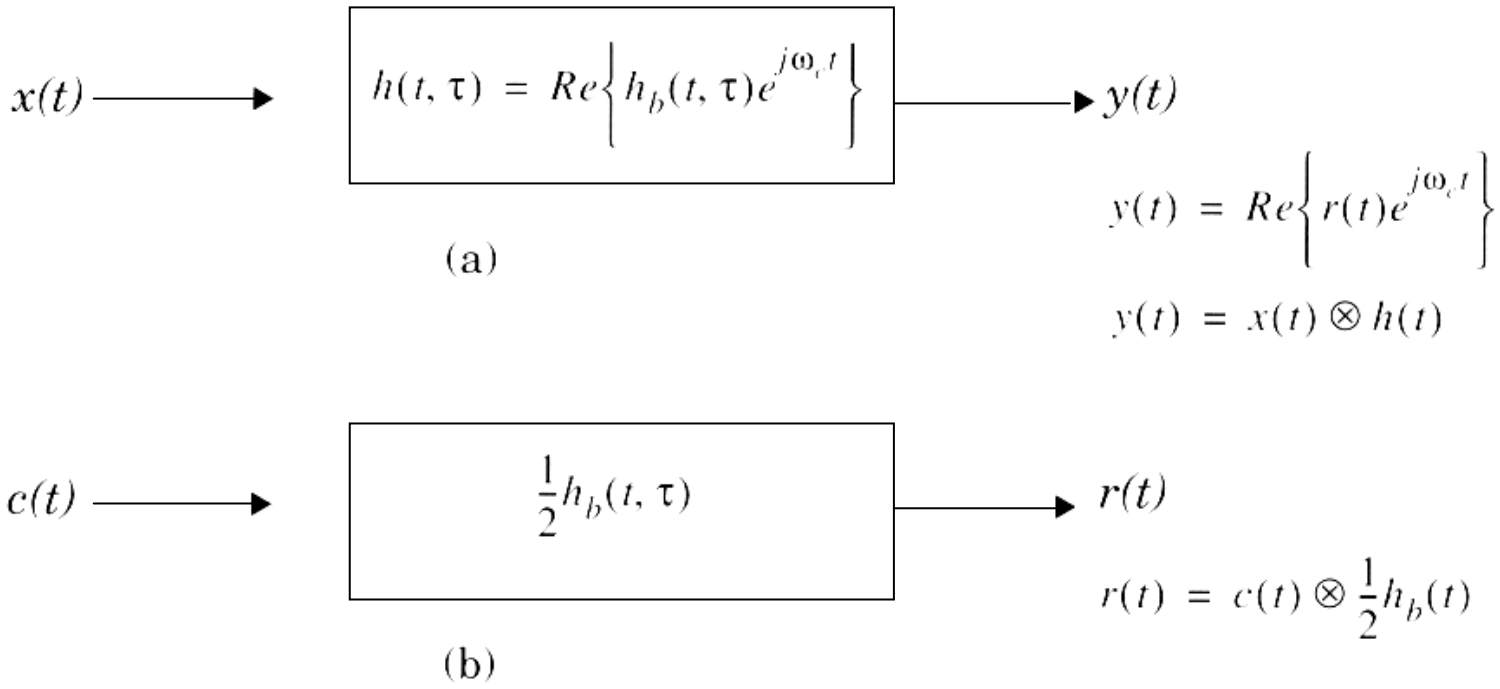

Figure 5.3 (a) Bandpass channel impulse response model; (b) baseband equivalent channel impulse response model.

Time-varying impulse response

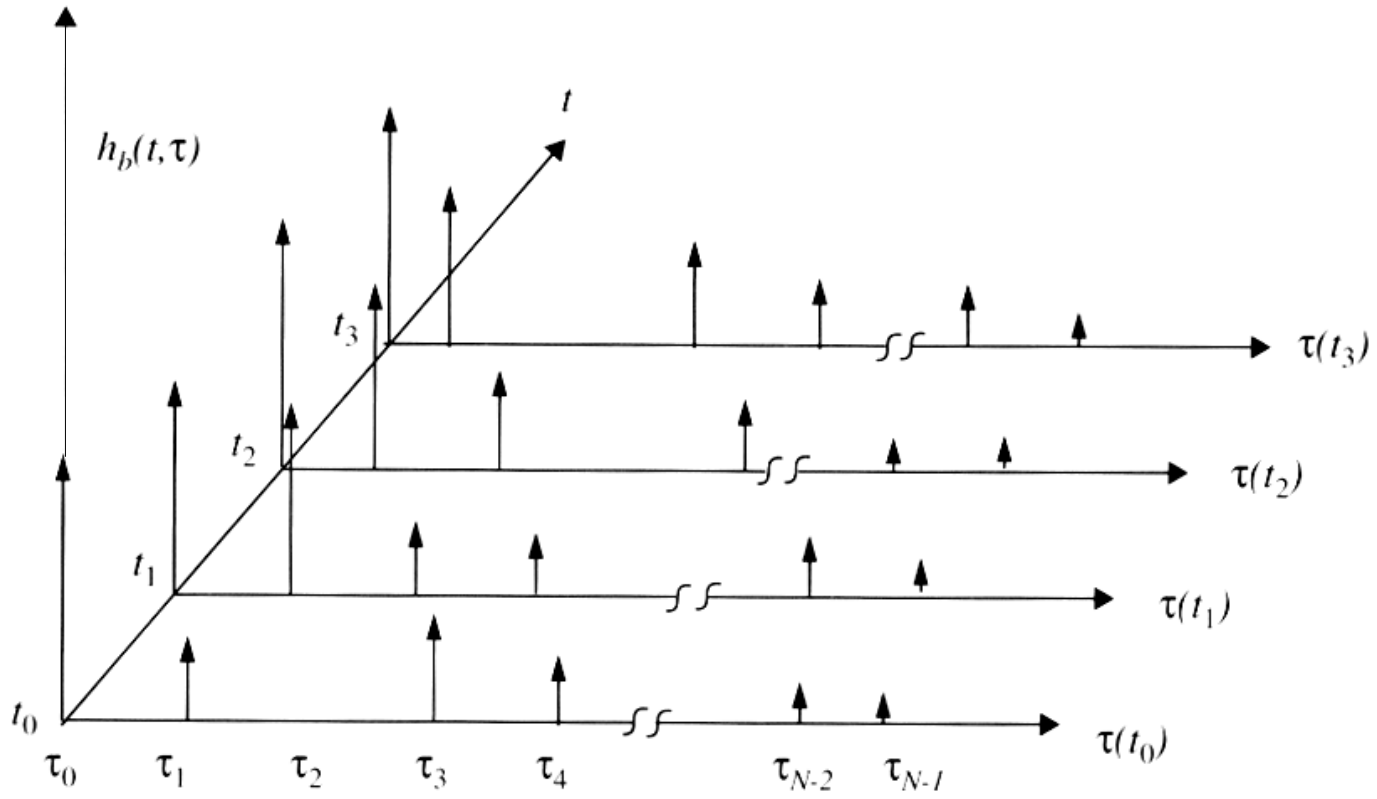

Figure 5.4 An example of the time varying discrete-time impulse response model for a multipath radio channel. Discrete models are useful in simulation where modulation data must be convolved with the channel impulse response [Tra02].

Impulse Response Model of a Multipath Channel

- Time-varying

$$h_b(t,\tau) = \sum_{i=0}^{N-1} \alpha_i(t,\tau) e^{(-j2\pi f_c \tau_i(t) + \phi_i(t,\tau))} \delta(\tau - \tau_i(t))$$

- Time-invariant

$$h_b(\tau) = \sum_{i=0}^{N-1} \alpha_i(\tau) e^{(-j\theta_i)} \delta(\tau - \tau_i)$$

Measured impulse responses

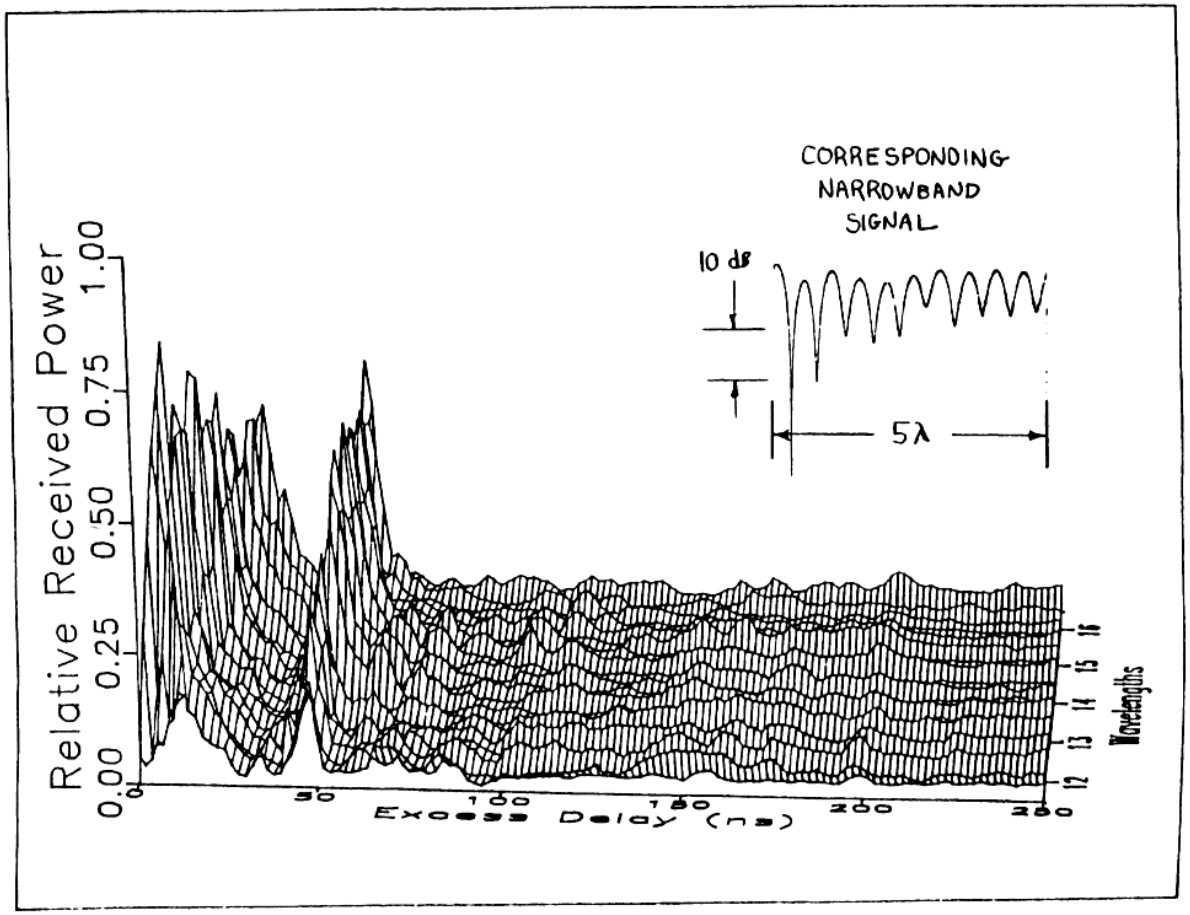

Figure 5.5 Measured wideband and narrowband received signals over a 5λ (0.375 m) measurement track inside a building. Carrier frequency is 4 GHz. Wideband power is computed using Equation (5.19), which can be thought of as the area under the power delay profile. The axis into the page is distance (wavelengths) instead of time.

Channel Sounder: Pulse type

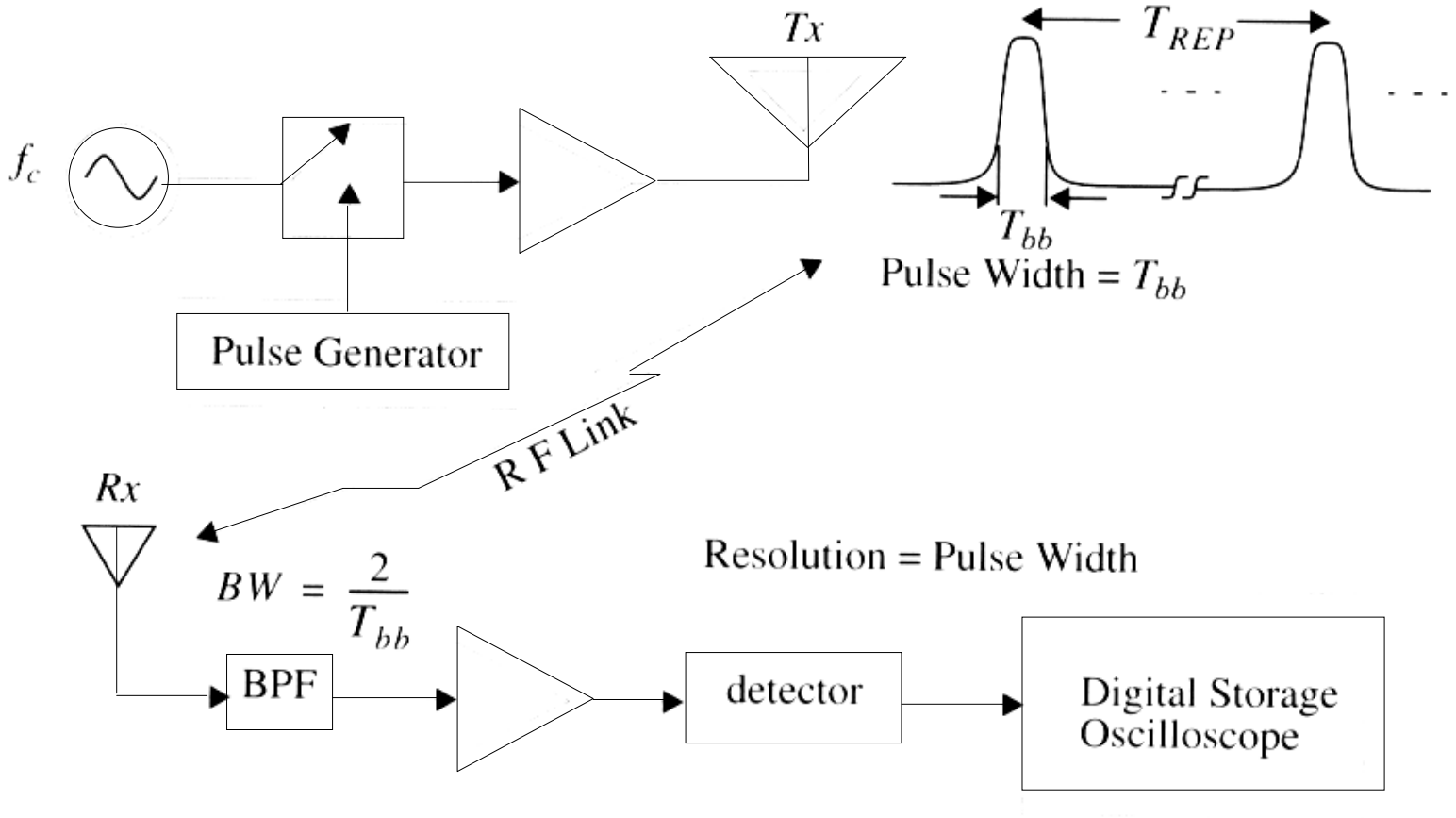

Figure 5.6 Direct RF channel impulse response measurement system.

Channel Sounder: PN Type

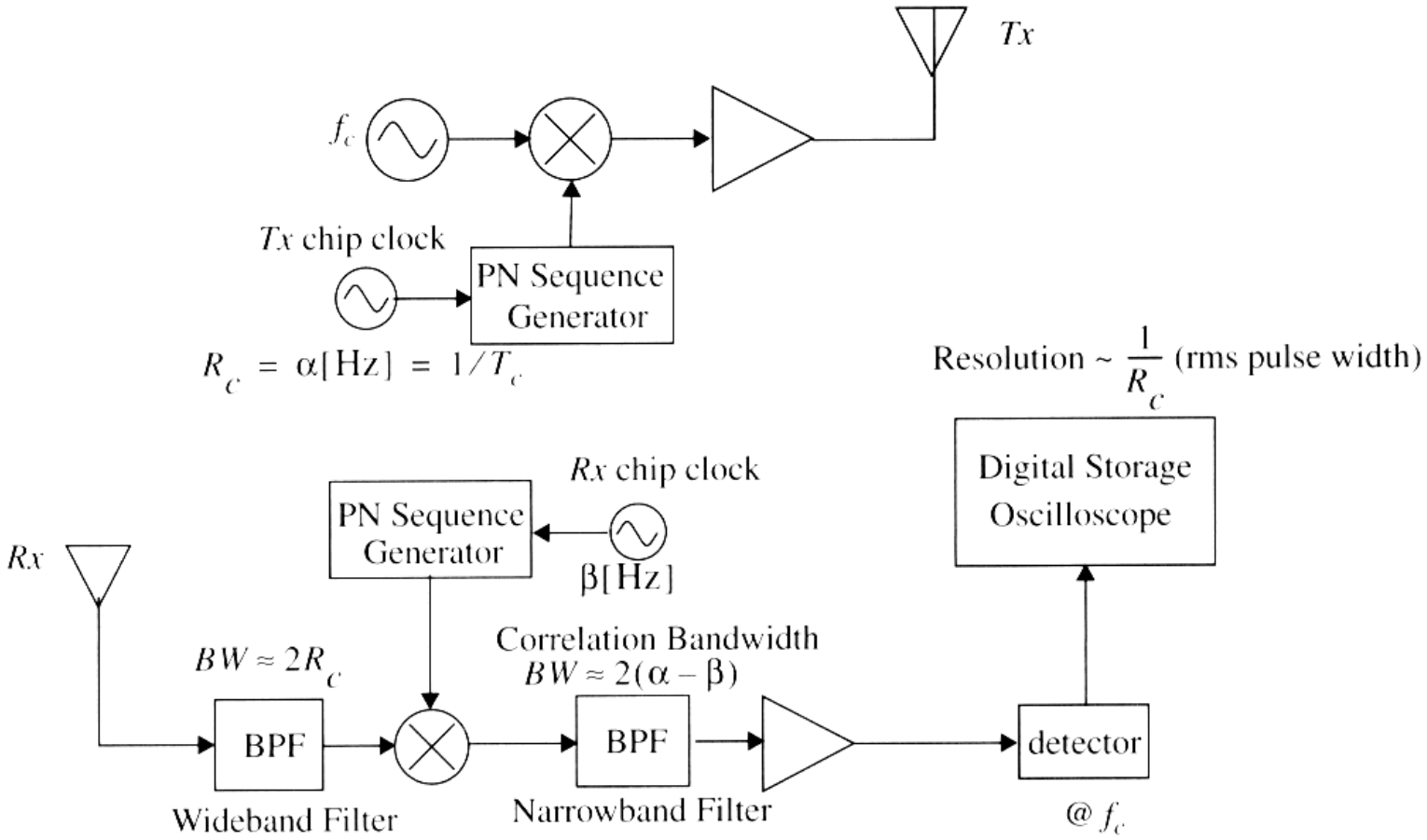

Figure 5.7 Spread spectrum channel impulse response measurement system.

Channel Sounder: Swept Freq. type

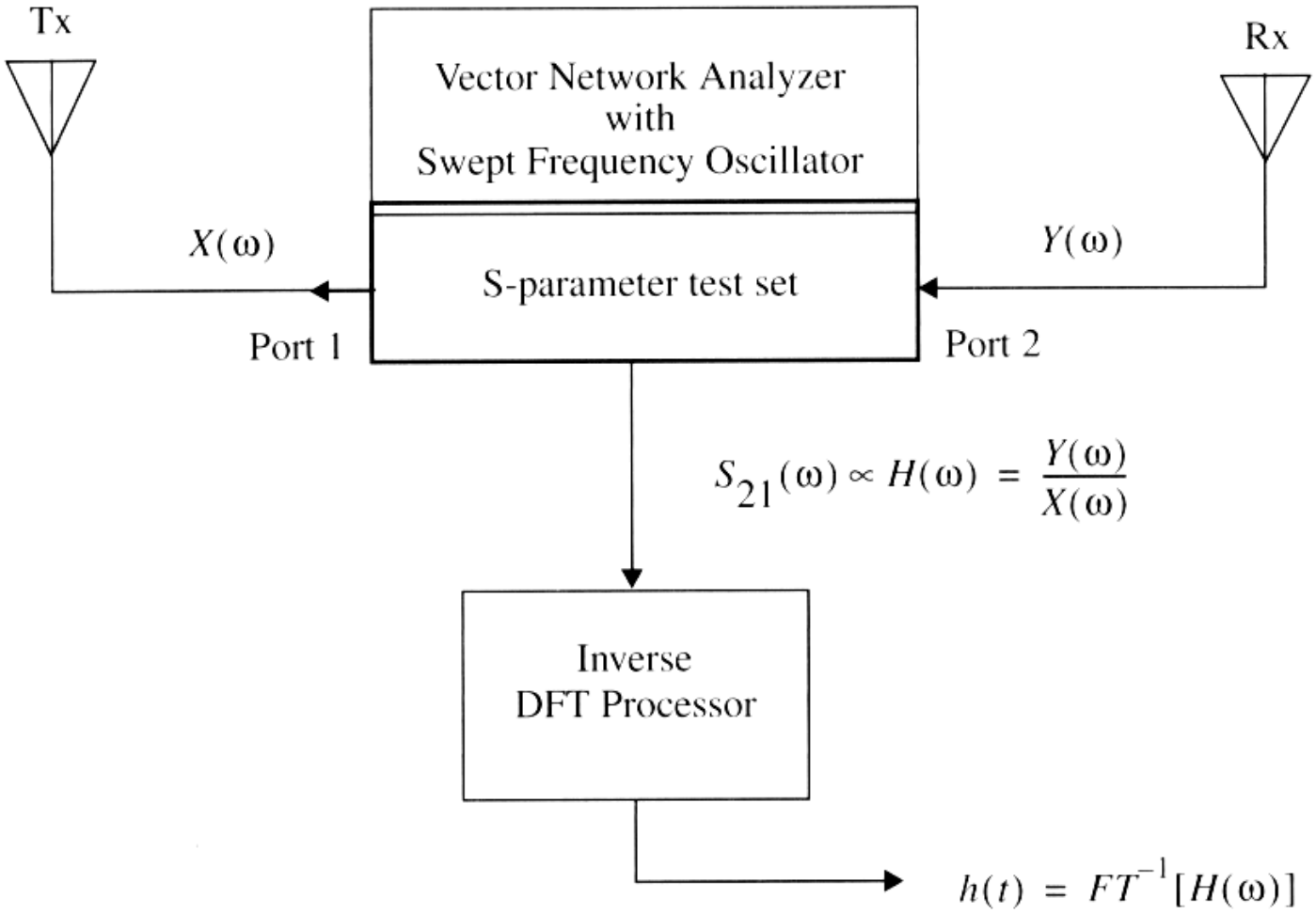

Figure 5.8 Frequency domain channel impulse response measurement system.

Measured power delay profiles

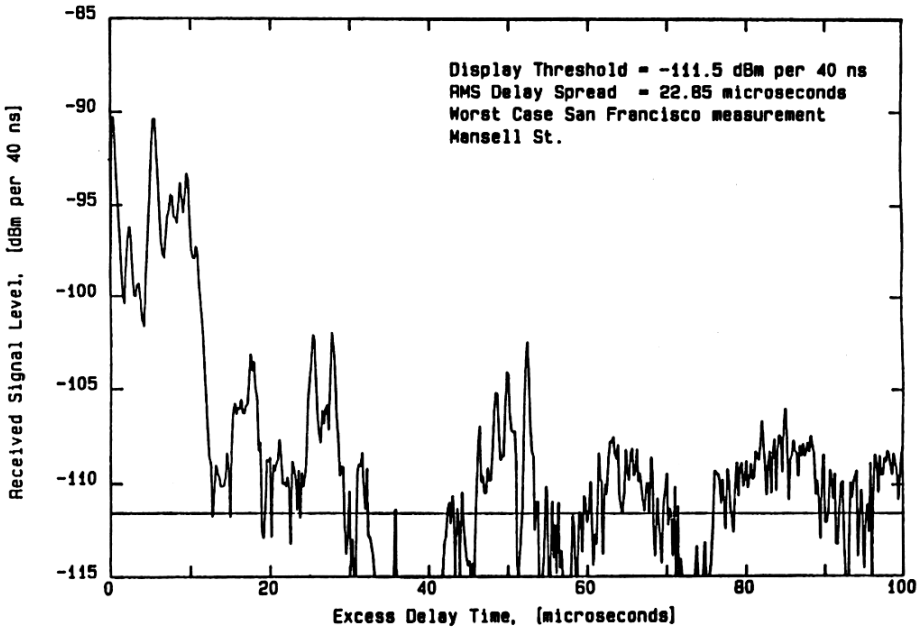

(a)

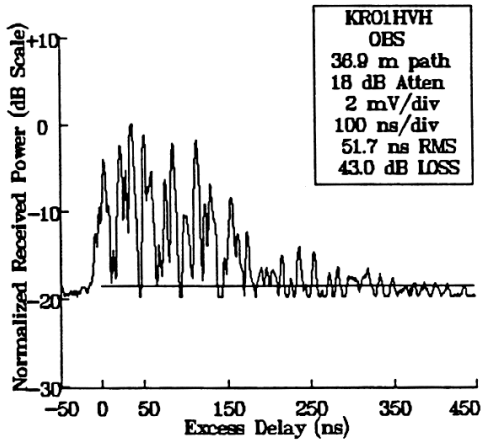

(b)

Figure 5.9 Measured multipath power delay profiles: a) From a 900 MHz cellular system in San Francisco [from [Rap90] © IEEE]; b) inside a grocery store at 4 GHz [from [Haw91] © IEEE].

Indoor Power Delay Profile

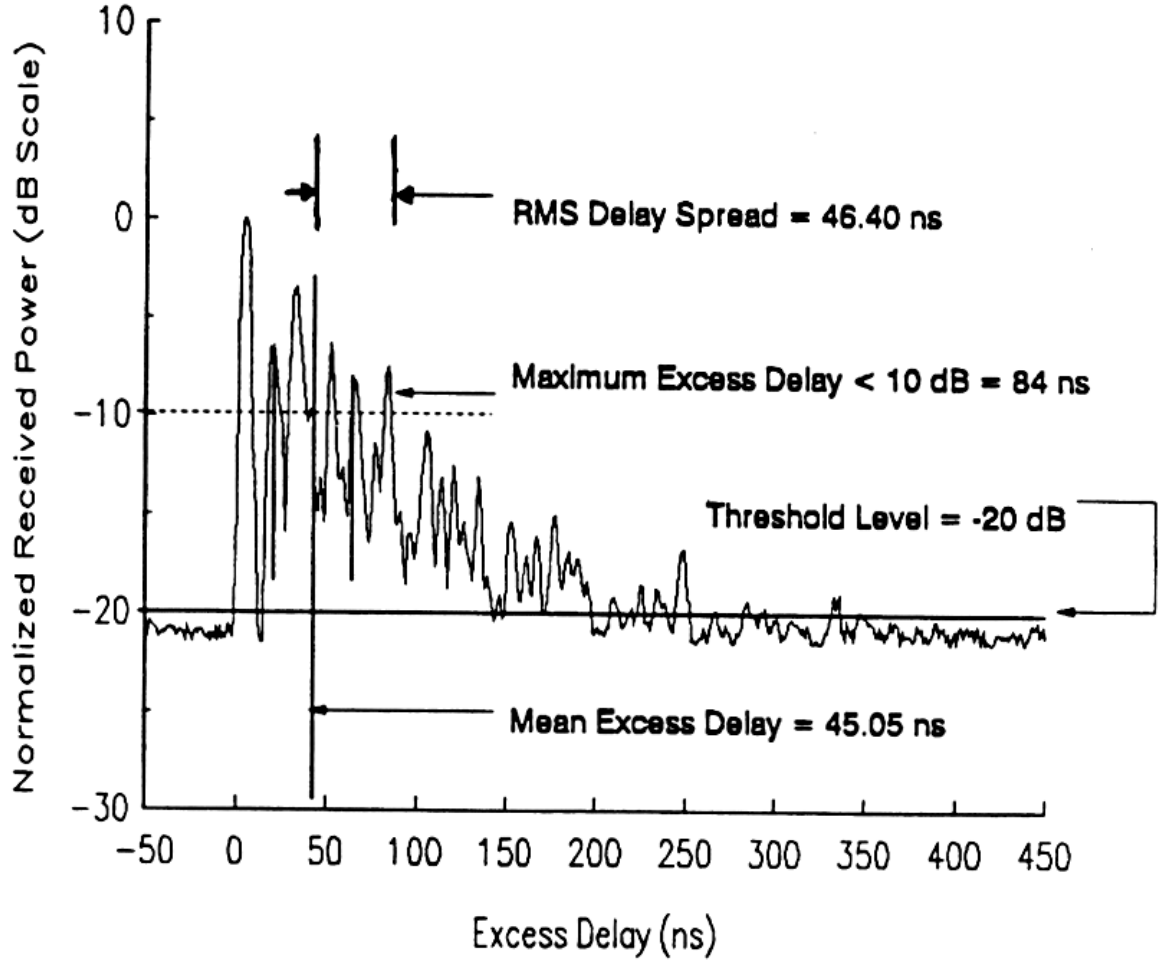

Figure 5.10 Example of an indoor power delay profile; rms delay spread, mean excess delay, maximum excess delay (10 dB), and threshold level are shown.

Typical RMS delay spreads

Table 5.1 Typical Measured Values of RMS Delay Spread

Environment	Frequency (MHz)	RMS Delay Spread (σ_τ)	Notes	Reference
Urban	910	1300 ns avg. 600 ns st. dev. 3500 ns max.	New York City	[Cox75]
Urban	892	10–25 μs	Worst case San Francisco	[Rap90]
Suburban	910	200–310 ns	Averaged typical case	[Cox72]
Suburban	910	1960–2110 ns	Averaged extreme case	[Cox72]
Indoor	1500	10–50 ns 25 ns median	Office building	[Sal87]
Indoor	850	270 ns max.	Office building	[Dev90a]
Indoor	1900	70–94 ns avg. 1470 ns max.	Three San Francisco buildings	[Sei92a]

Time Dispersion parameters

- Mean excess delay

$$\bar{\tau} = \frac{\sum_k \alpha_k^2 \tau_k}{\sum_k \alpha_k^2} = \frac{\sum_k P(\tau_k)\tau_k}{\sum_k P(\tau_k)}$$

- rms delay spread

$$\sigma_\tau = \sqrt{\overline{\tau^2} - (\bar{\tau})^2}, \text{ where } \overline{\tau^2} = \frac{\sum_k \alpha_k^2 \tau_k^2}{\sum_k \alpha_k^2} = \frac{\sum_k P(\tau_k)\tau_k^2}{\sum_k P(\tau_k)}.$$

- Maximum delay spread (X dB)
  - The time delay during which multipath energy falls to X dB below the maximum.

Coherence bandwidth & Coherence time

- **Coherence bandwidth**:
  - Coherence bandwidth is a statistical measure of the range of frequencies over which the channel can be considered “flat”. In other words, Coherence bandwidth is the range of frequencies over which any two frequency components experience strongly correlated fading.
  - In wireless communications the maximum difference of the arrival time between the first arrival multipath replica and the last multipath replica determines the coherence bandwidth of the wireless channel.
  - $$B_c \propto \frac{1}{\sigma_\tau}$$
- **Coherence time**:
  - Coherence time is a statistical measure of the time duration over which the channel impulse response is essentially invariant. In other words, Coherence time is the time duration over which two received signals have a strong potential for amplitude correlation.
  - In wireless communications the maximum Doppler spread determines the coherence time of the channel.
  - $$T_c \propto \frac{1}{f_m}, \ f_m \text{ is the maximum Doppler spread.}$$

Two independent fading issues

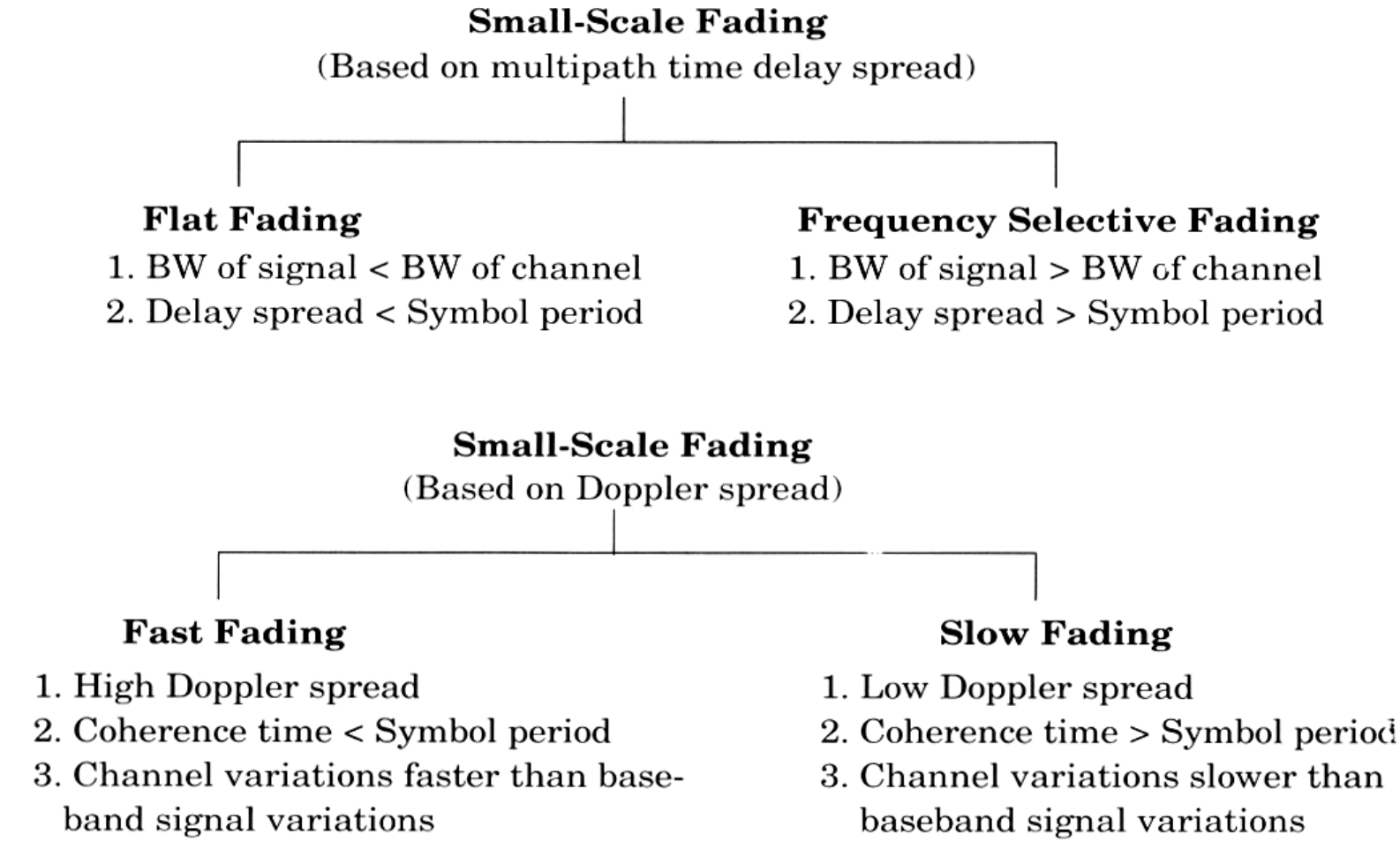

Figure 5.11 Types of small-scale fading.

Flat-fading (non-freq. Selective)

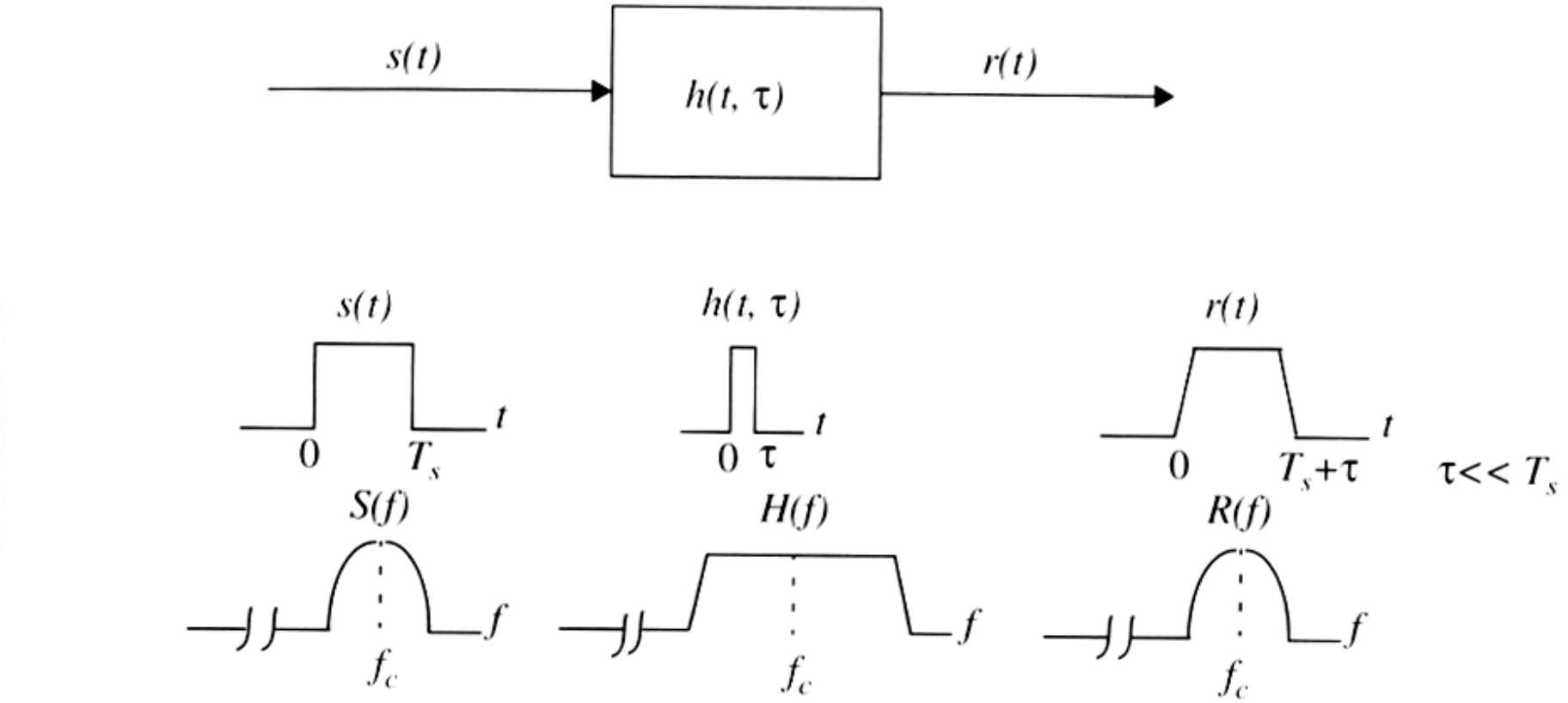

Figure 5.12 Flat fading channel characteristics.

Frequency selective fading

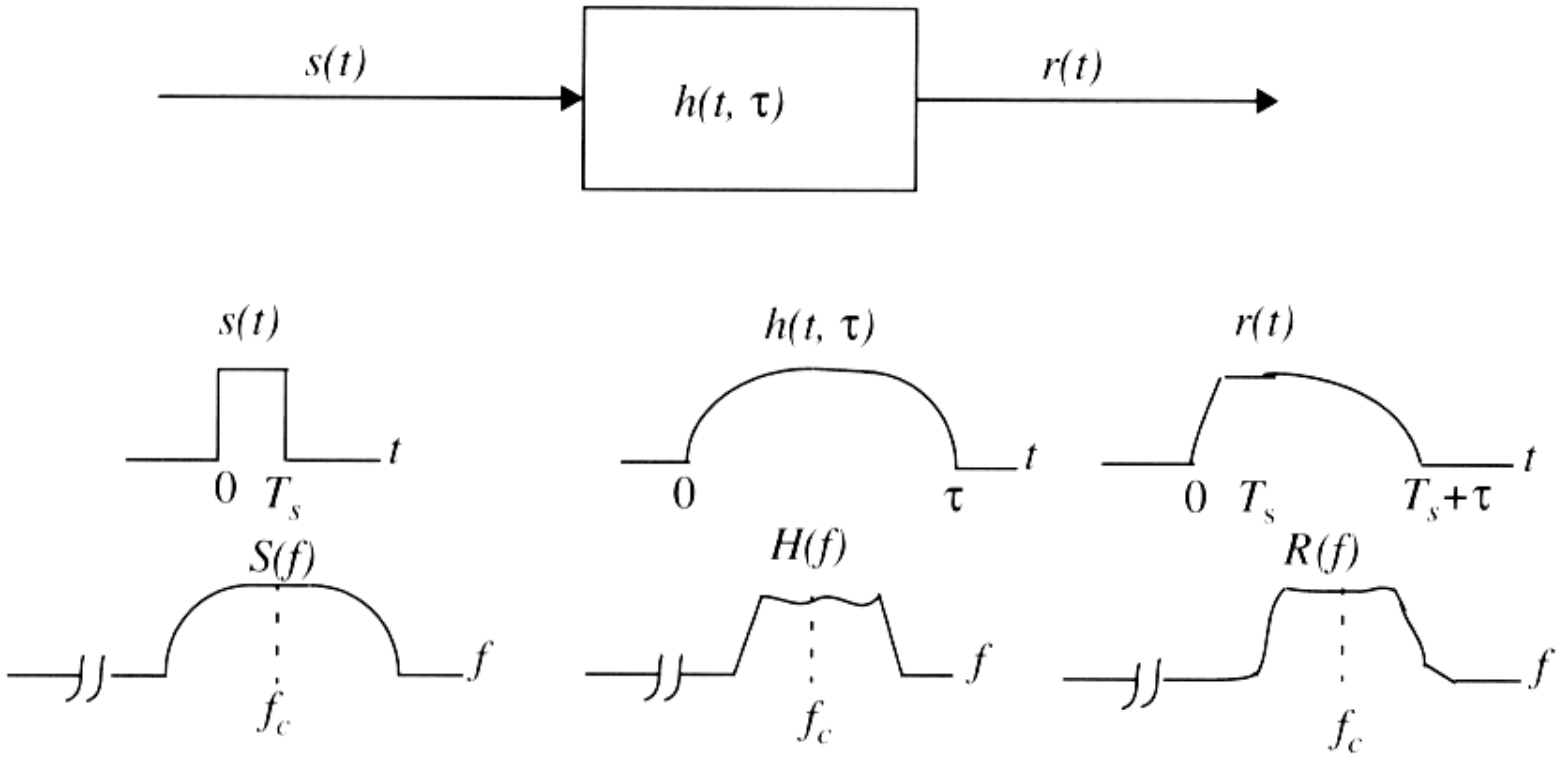

Figure 5.13 Frequency selective fading channel characteristics.

Two independent fading issues

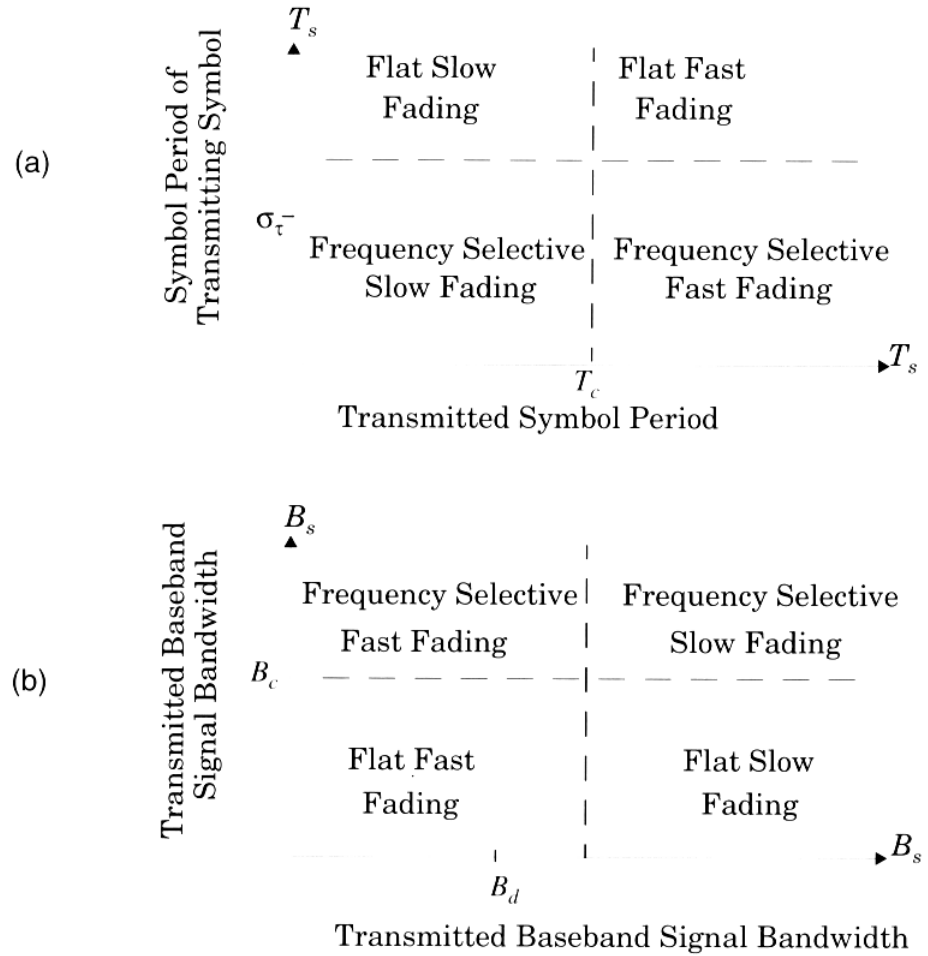

Figure 5.14 Matrix illustrating type of fading experienced by a signal as a function of: (a) symbol period; and (b) baseband signal bandwidth.

Rayleigh fading

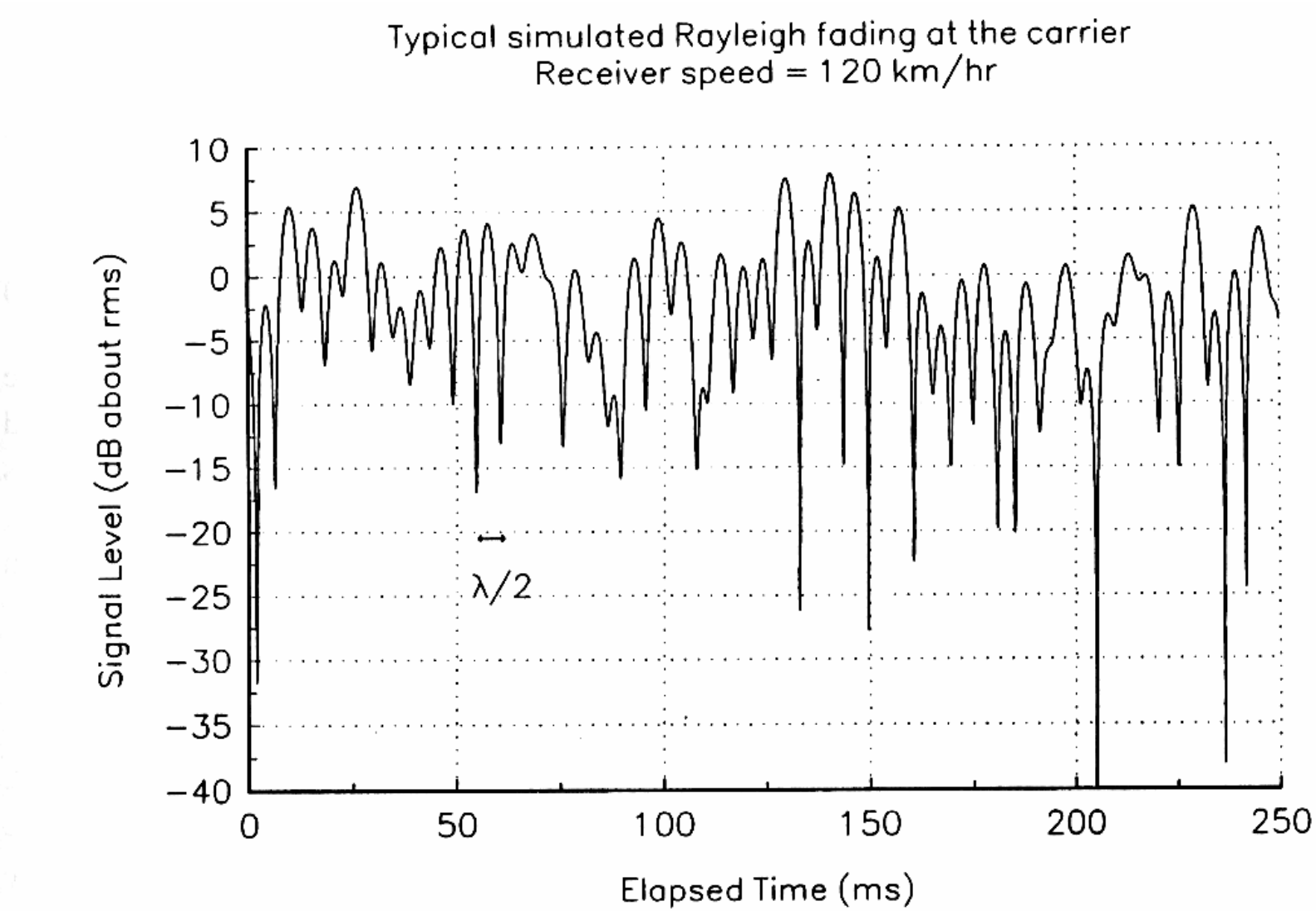

Figure 5.15 A typical Rayleigh fading envelope at 900 MHz [from [Fun93] © IEEE].

Rayleigh fading Distribution

- Probability Density Function (PDF)

$$p(r) = \begin{cases} \dfrac{r}{\sigma^2} e^{\left(-\frac{r^2}{2\sigma^2}\right)} & (0 \le r < \infty) \\ 0 & (r < 0) \end{cases}$$

- Cumulative Density Function (CDF)

$$P(R) = 1 - e^{\left(-\frac{R^2}{2\sigma^2}\right)}$$

Ricean Fading Distribution

- A dominant stationary (nonfading) signal component present, such as a line-of sight propagation path.
- Probability Density Function (PDF)

$$\bullet\ p(r) = \begin{cases} \dfrac{r}{\sigma^2} e^{\left(-\frac{(r^2+A^2)}{2\sigma^2}\right)} I_0\left(\dfrac{Ar}{\sigma^2}\right) & \text{for } (A \geq 0, r \geq \infty) \\ 0 & \text{for } (r < 0) \end{cases}$$

$$where\ I_0 \text{ is the bessel function of the first kind and zero - order}$$

$$\bullet\ K(dB) = 10\log\frac{A^2}{2\sigma^2} dB$$

- The Ricean distribution is often described in terms of a parameter K.

Small-scale envelope distributions

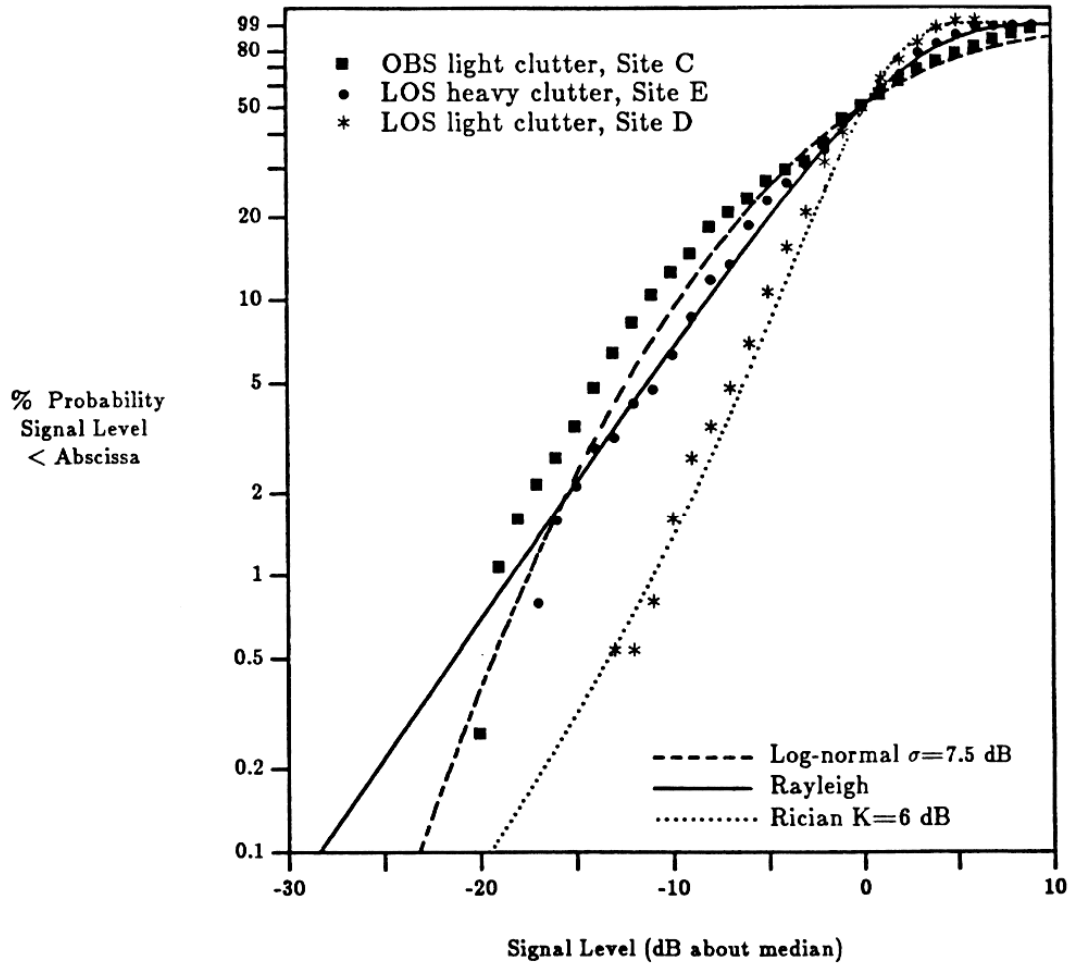

Figure 5.17 Cumulative distribution for three small-scale fading measurements and their fit to Rayleigh, Ricean, and log-normal distributions [from [Rap89] © IEEE].

Ricean and Rayleigh fading distributions

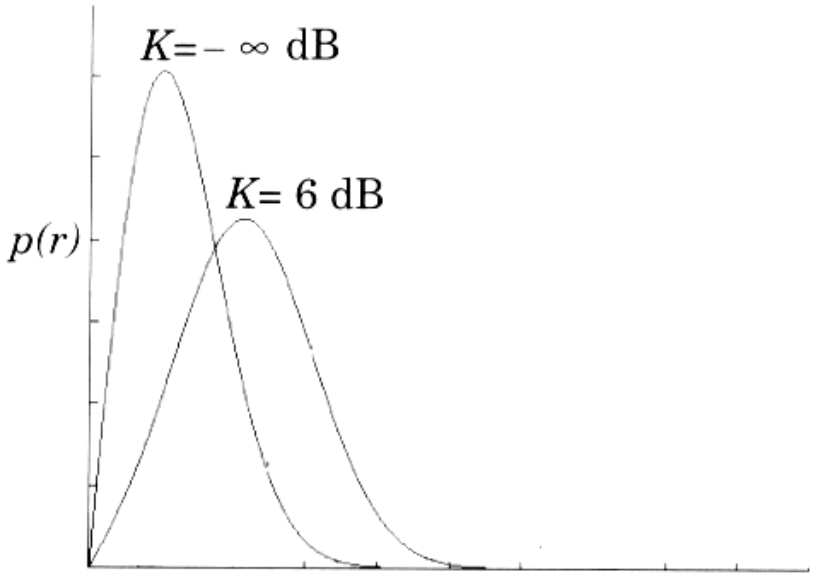

Figure 5.18 Probability density function of Ricean distributions: $K = -\infty$ dB (Rayleigh) and $K = 6$ dB. For K >> 1, the Ricean pdf is approximately Gaussian about the mean.

Small-scale fading mechanism

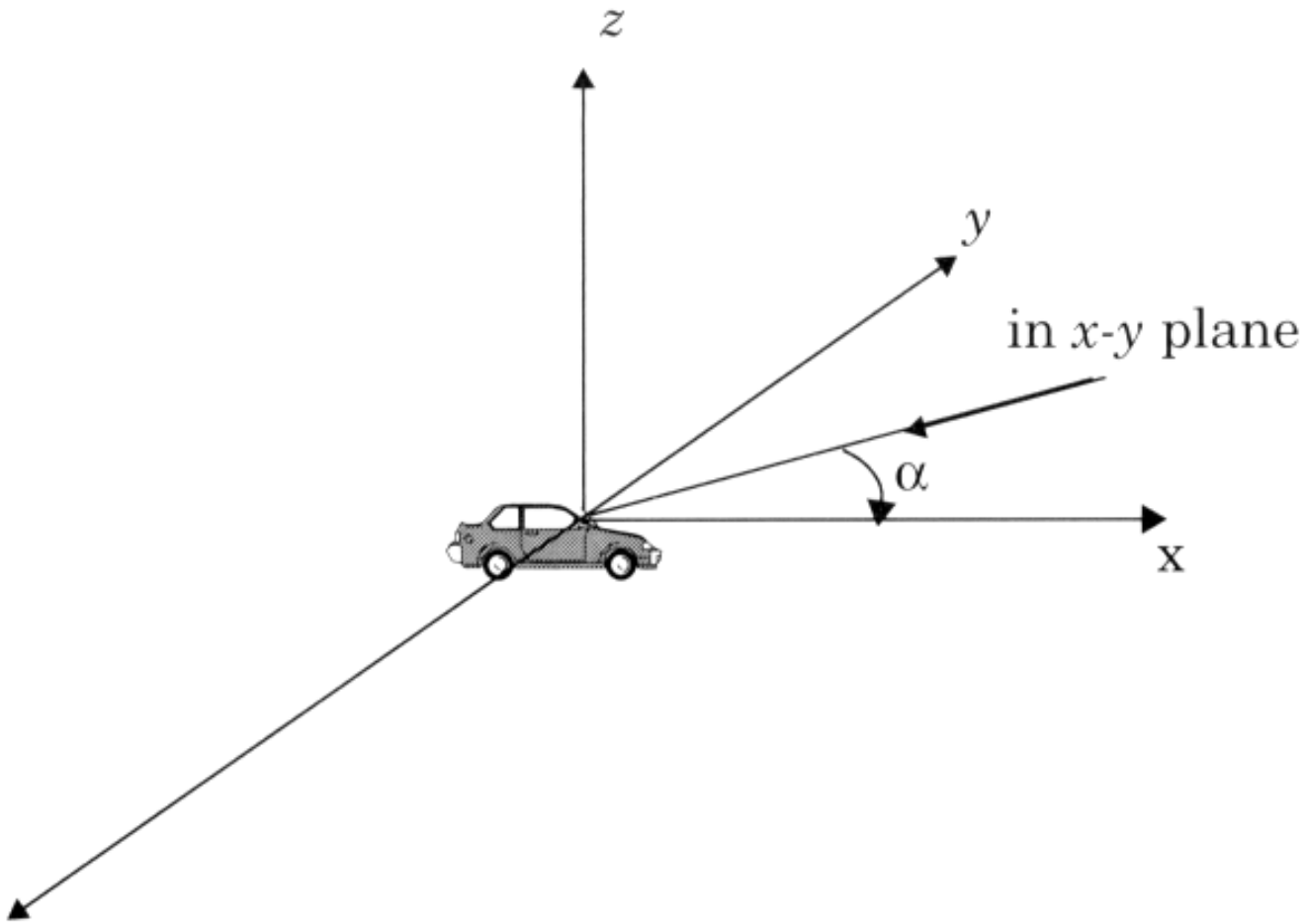

Figure 5.19 Illustrating plane waves arriving at random angles.

Channel modeling

- Jake's model
  - See handout
- Modified Jake's model
  - See handout

Doppler effect

- We have $f_d(\alpha_n) = f_m \cos\alpha_n$.
- Assuming that α_n is uniformly distributed.
- The received power in angle $|d\alpha_n|$ around α_n is given by $G(\alpha_n)p(\alpha_n)|d\alpha_n|$, where the absolute operation is due to the fact that power is always positive, and
  - $G(\alpha_n)$ represents the average power in correspondence with an angle.
  - $p(\alpha_n) = \frac{1}{2\pi}$
- Notice that both α_n and $-\alpha_n$ generate the same Doppler frequency f_d.

Doppler effect'

- Hence, the Doppler power spectral density $S(f_d)$ can be computed using the Parseval's theorem by equating the incident received power $(G(\alpha_n)p(\alpha_n)+G(-\alpha_n)p(-\alpha_n))|d\alpha_n|$ with the power $S(f_d)|df_d|$ (power is positive), yielding

$$S(f_d)|df_d| = (G(\alpha_n)p(\alpha_n)+G(-\alpha_n)p(-\alpha_n))|d\alpha_n|$$

- From $f_d(\alpha_n) = f_m \cos\alpha_n$, we may obtain

$$|df_d| = f_m|-\sin\alpha_n||d\alpha_n|$$

where from $\cos\alpha_n = f_d / f_m$ and $\sin^2\alpha_n + \cos^2\alpha_n = 1$, we have

$$\sin\alpha_n = \sqrt{1-\left(\frac{f_d}{f_m}\right)^2}$$

Doppler effect''

- It can be shown that

$$S(f_d) = \frac{G(\alpha_n)\,p(\alpha_n) + G(-\alpha_n)\,p(-\alpha_n)}{f_m\sqrt{1-\left(\frac{f_d}{f_m}\right)^2}}$$

$$= \frac{C}{2\pi f_m\sqrt{1-\left(\frac{f_d}{f_m}\right)^2}}$$

- The power spectrum $S(f_d)$ has a U-shape and

$$S(f_d = 0) = C \text{ and } S(f_d = f_m) = \infty.$$

Doppler spectrum

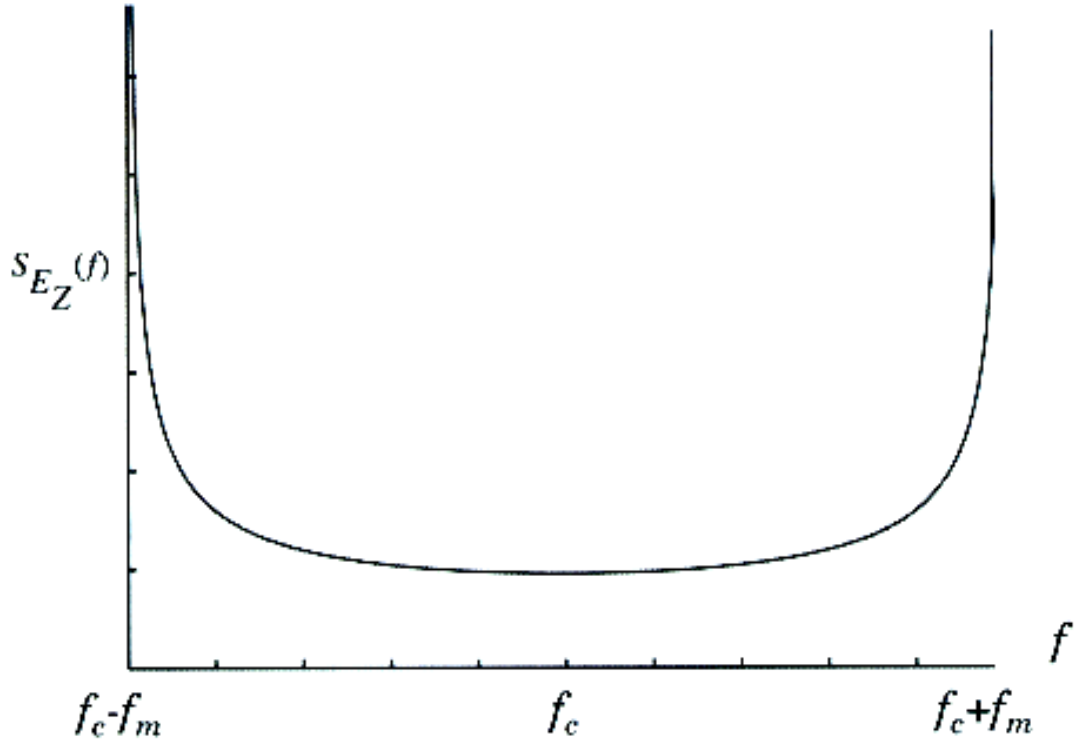

Figure 5.20 Doppler power spectrum for an unmodulated CW carrier [from [Gan72] © IEEE].

Spectrum of Envelope of Doppler faded signal

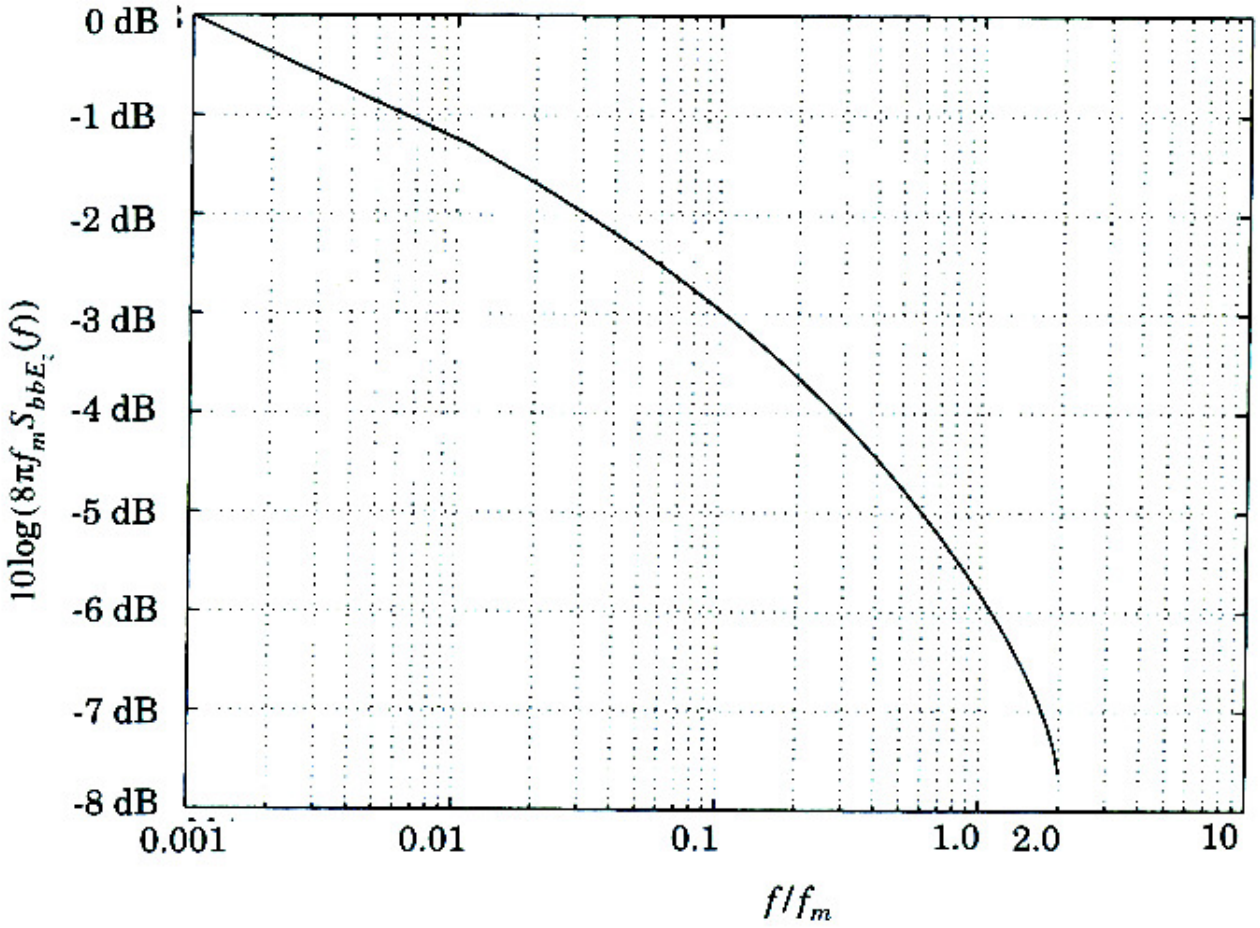

Figure 5.21 Baseband power spectral density of a CW Doppler signal after envelope detection.

Simulating Doppler/Small-scale fading

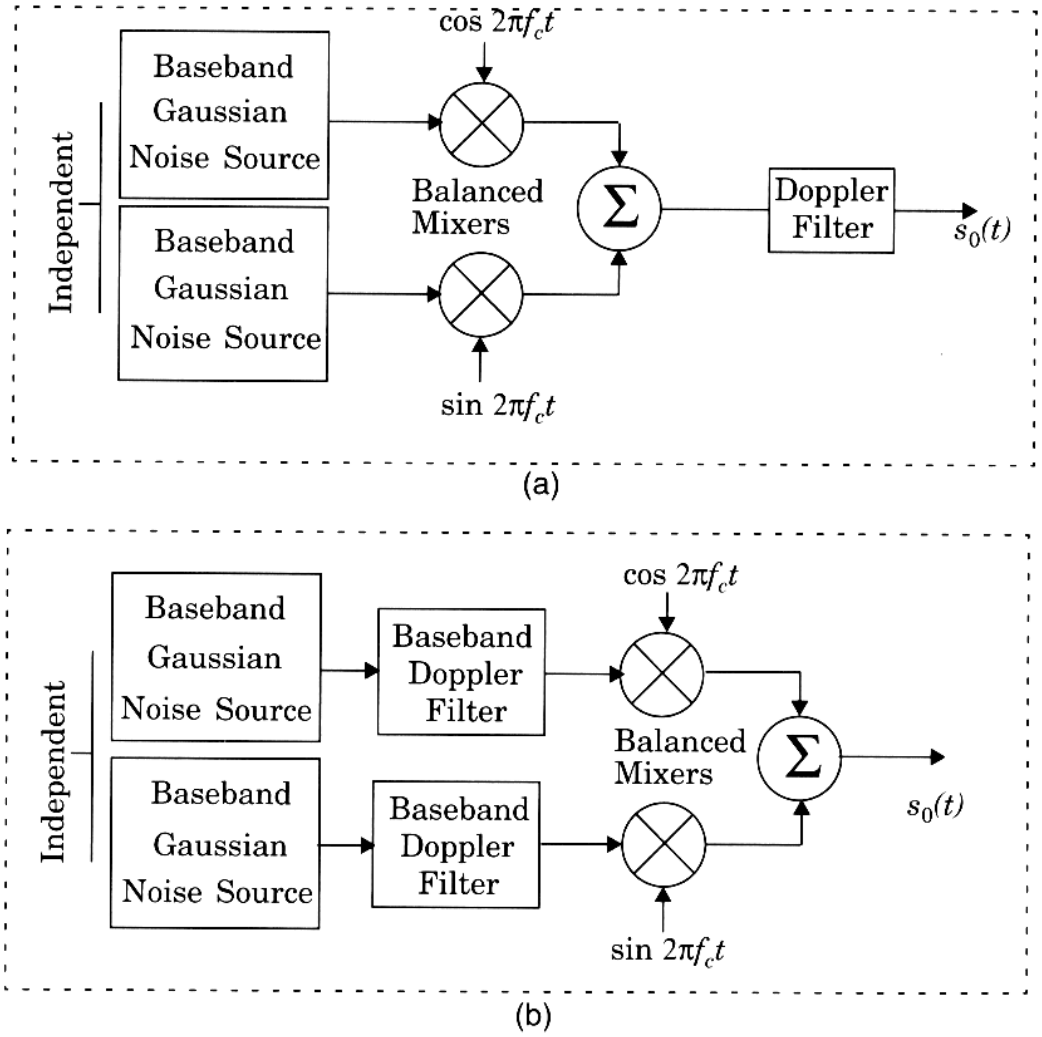

Figure 5.22 Simulator using quadrature amplitude modulation with (a) RF Doppler filter and (b) baseband Doppler filter.

Simulating Doppler fading

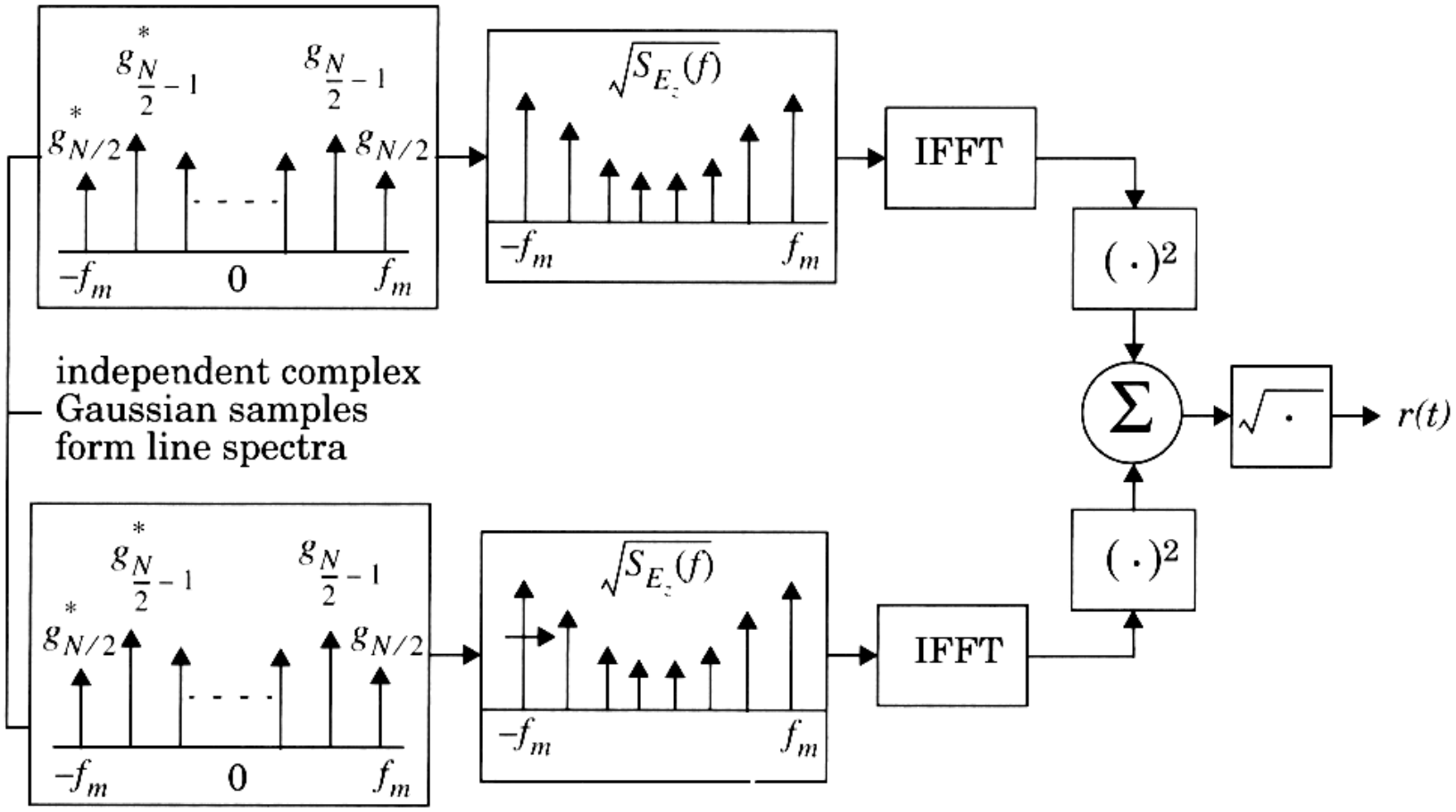

Figure 5.24 Frequency domain implementation of a Rayleigh fading simulator at baseband

Uncorrelated Rayleigh magnitude response

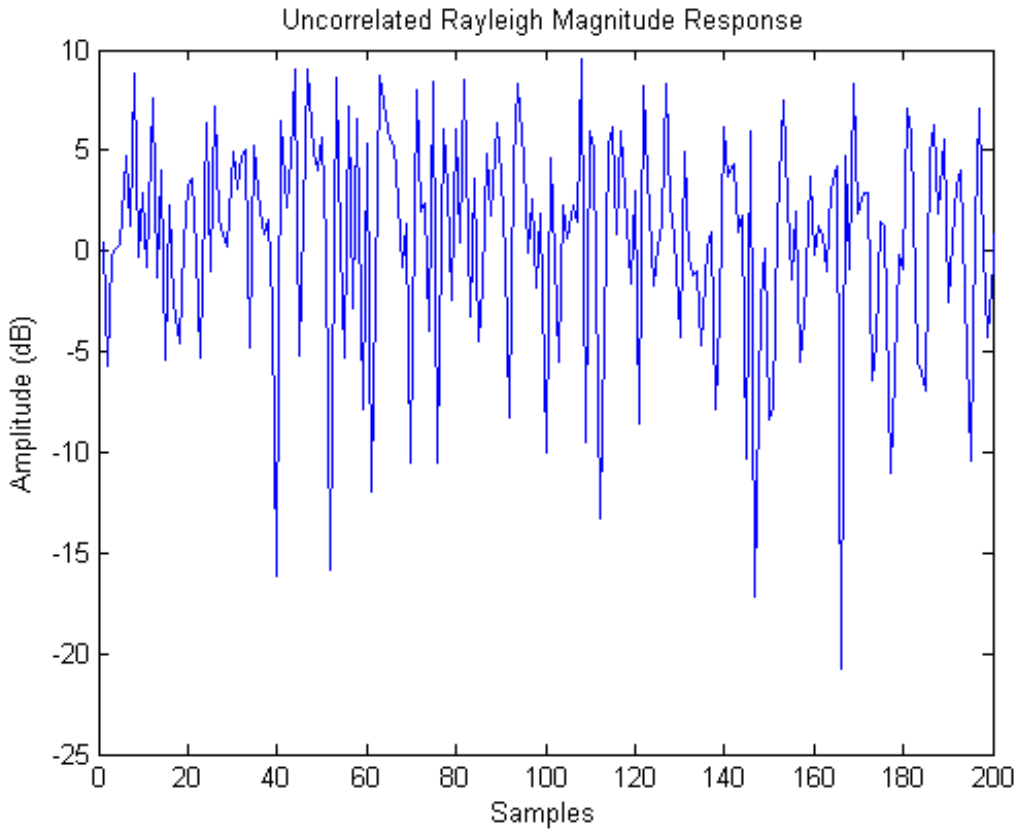

Details: 10^6 samples

Uncorrelated Rayleigh phase response

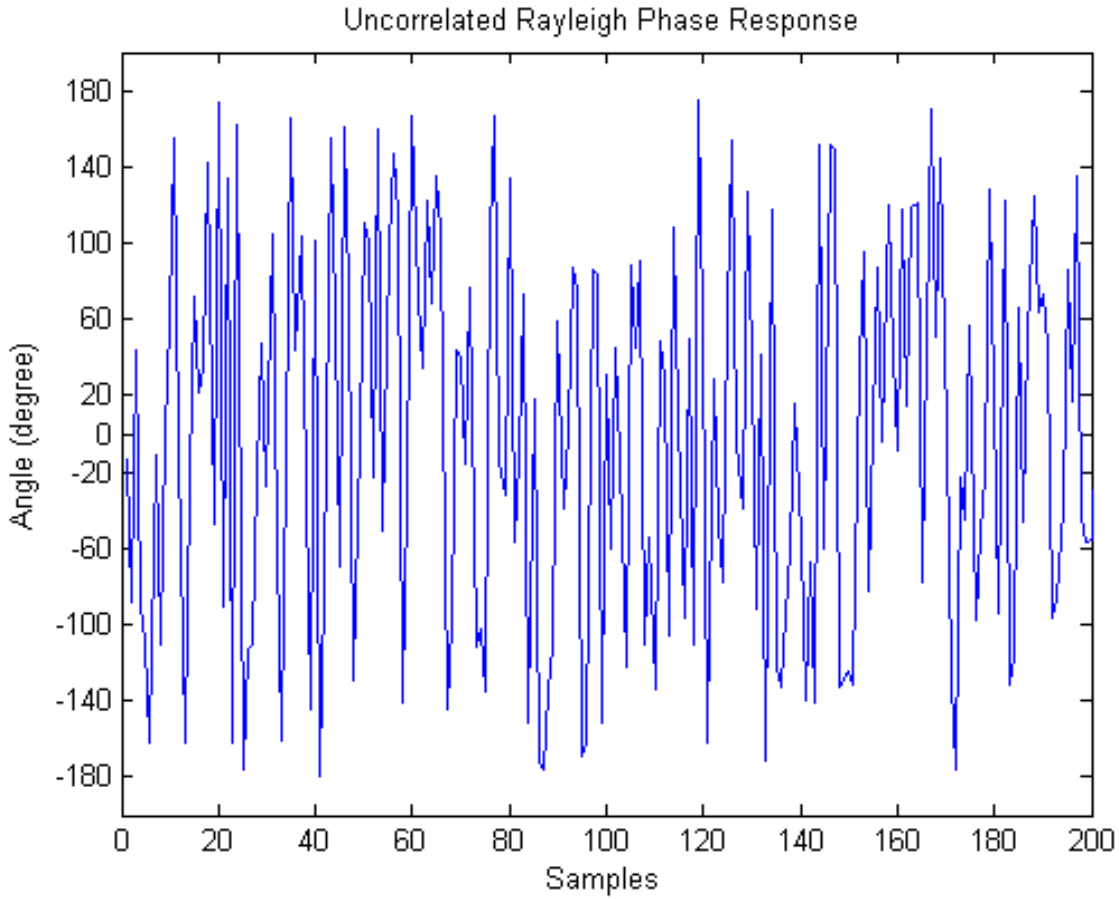

Details: 10^6 samples

Correlated Rayleigh magnitude response.

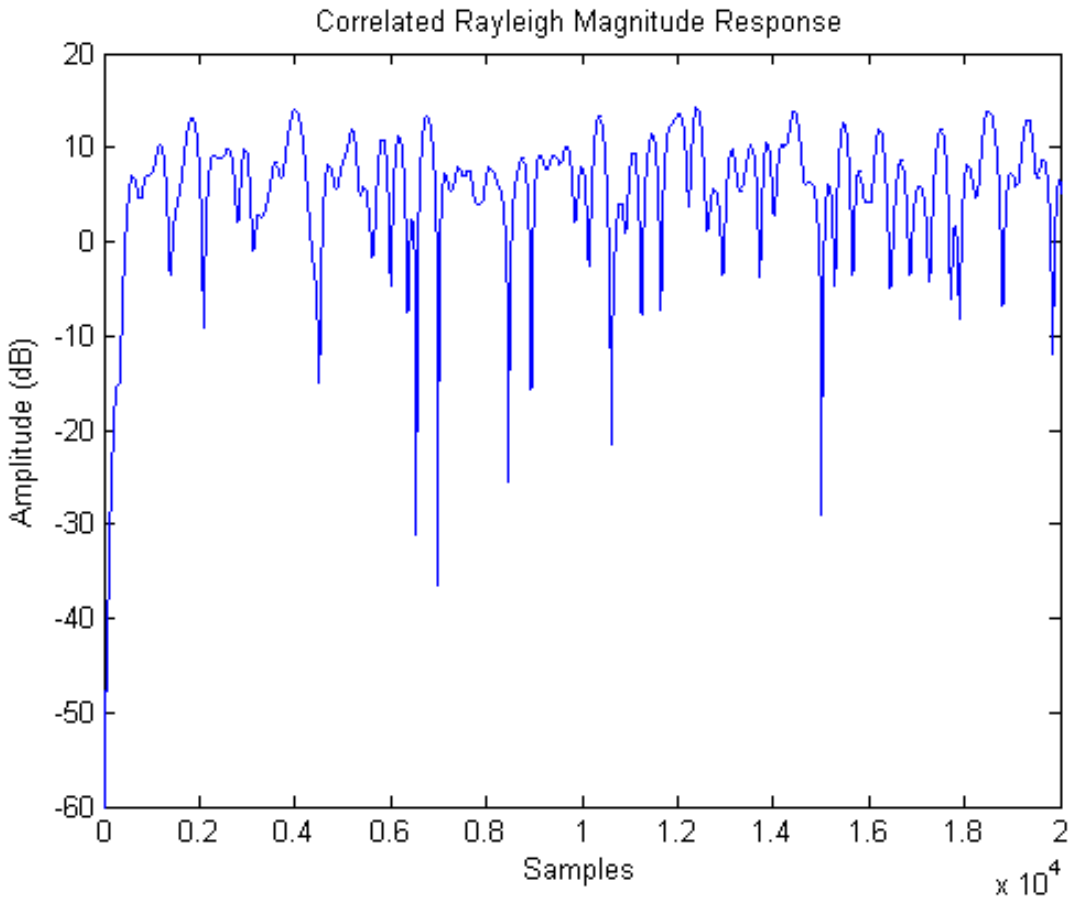

Details: 10^6 samples , filter order=1024 and fm=0.004)

Correlated Rayleigh phase response

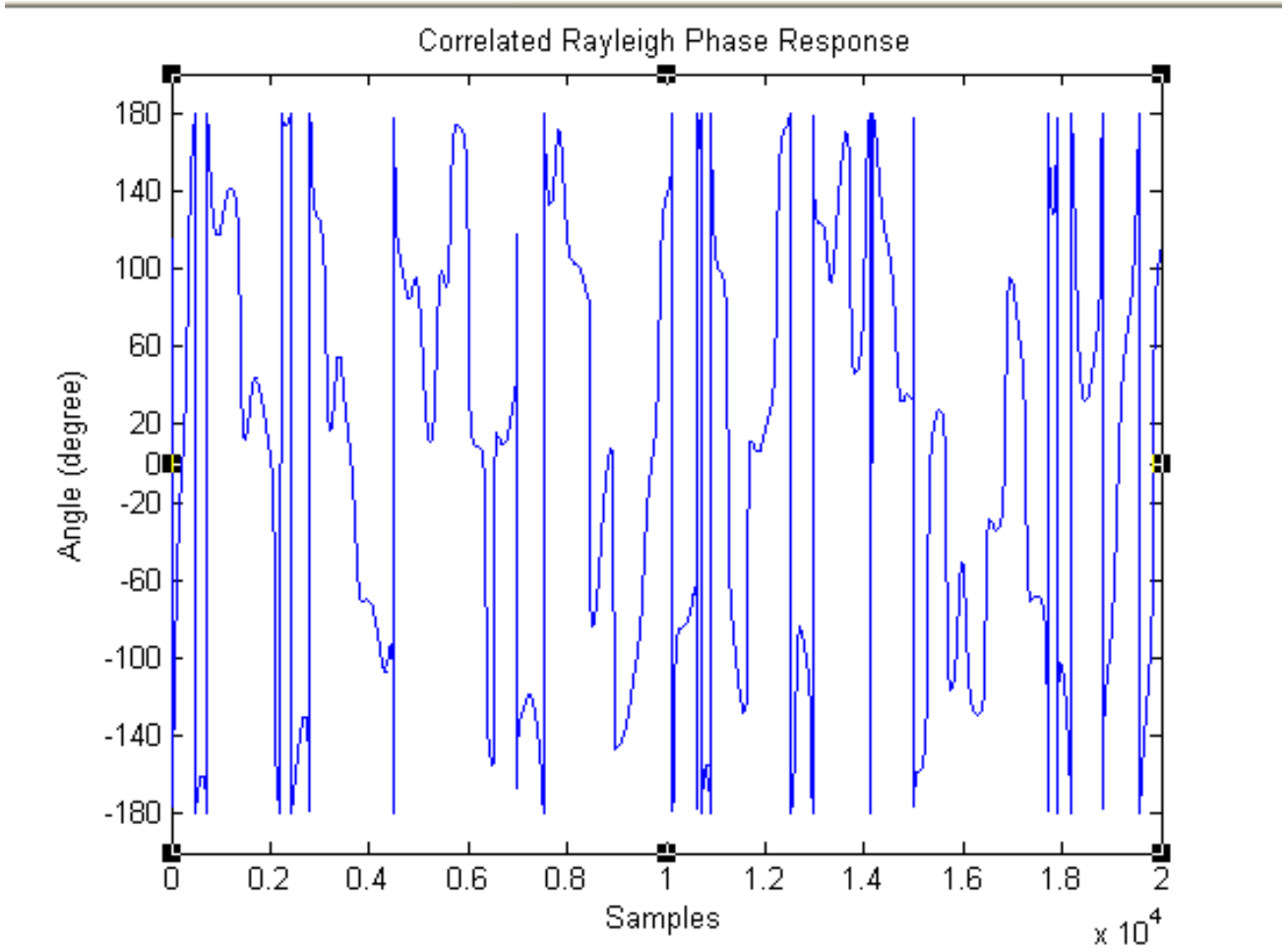

Details: 10^6 samples , filter order=1024 and fm=0.004)

Comparisons between the theoretical or uncorrelated Rayleigh PDF with simulation histogram with different maximum Doppler frequency

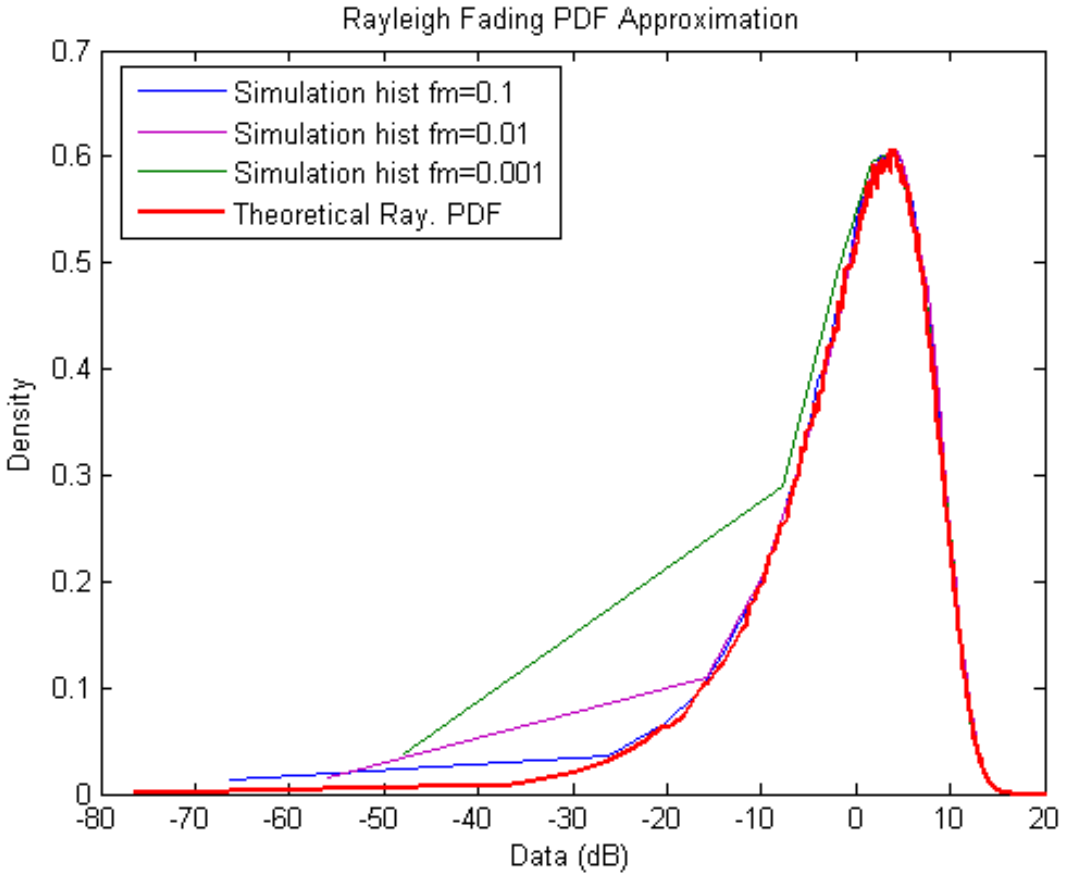

Details: 10^6 samples , filter order=1024 and fm=0.004)

Simulating multipath with Doppler-induced Rayleigh fading

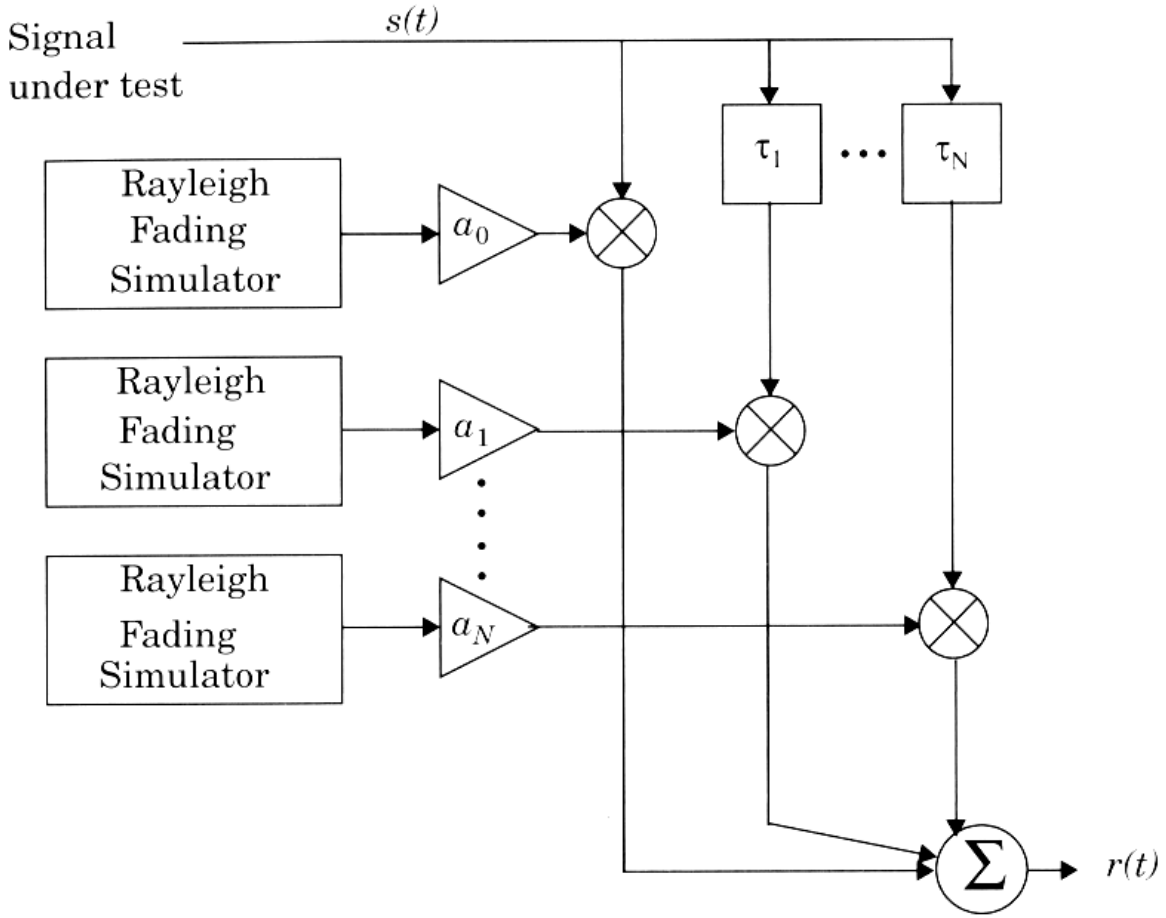

Figure 5.25 A signal may be applied to a Rayleigh fading simulator to determine performance in a wide range of channel conditions. Both flat and frequency selective fading conditions may be simulated, depending on gain and time delay settings.

Simulating 2-ray multipath

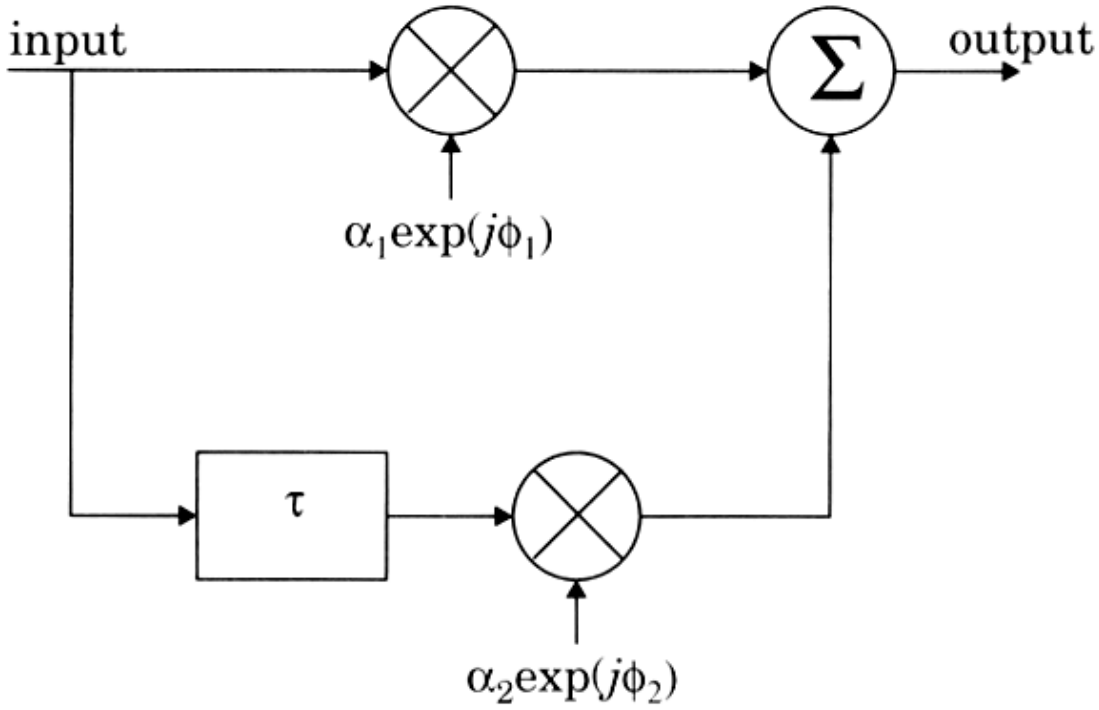

Figure 5.26 Two-ray Rayleigh fading model.

SIRCIM – Simulation of all indoor propagation Characteristics

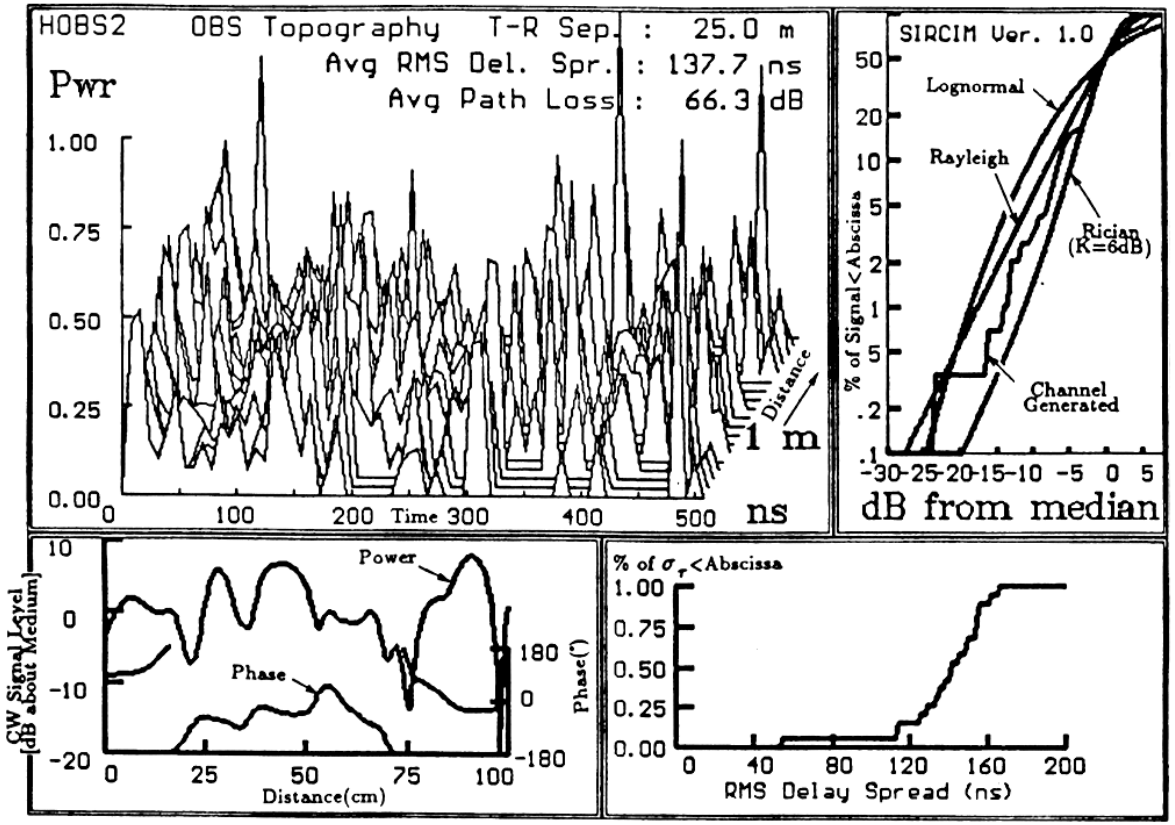

Figure 5.27 Indoor wideband impulse responses simulated by SIRCIM at 1.3 GHz. Also shown are the distributions of the rms delay spread and the narrowband signal power distribution. The channel is simulated as being obstructed in an open-plan building, T–R separation is 25 m. The rms delay spread is 137.7 ns. All multipath components and parameters are stored on disk [from [Rap93a] © IEEE].

SMRCIM – Simulation of all outdoor propagation Characteristics

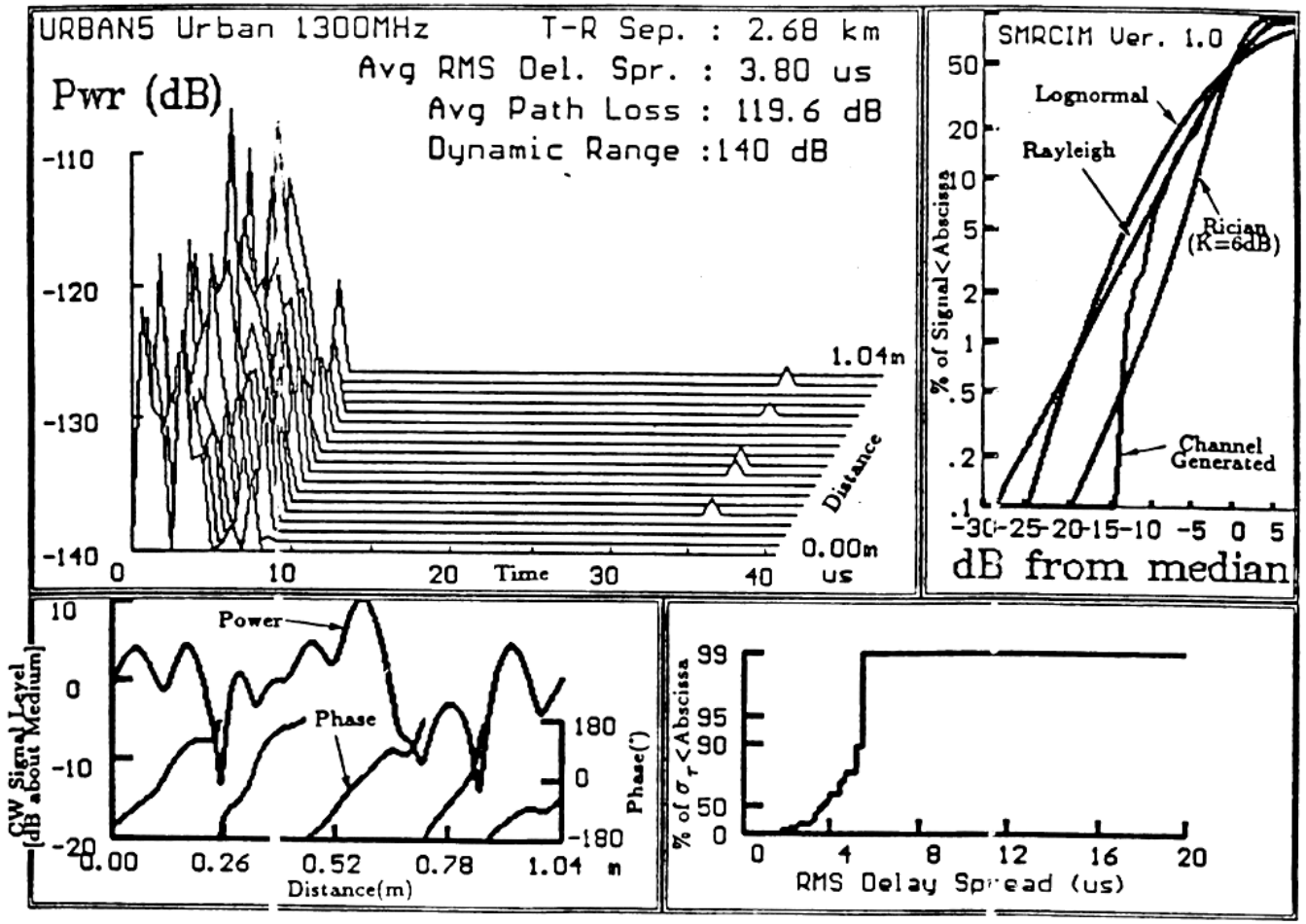

Figure 5.28 Urban wideband impulse responses simulated by SMRCIM at 1.3 GHz. Also shown are the distributions of the rms delay spread and the narrowband fading. T–R separation is 2.68 km. The rms delay spread is 3.8 μs. All multipath components and parameters are saved on disk. [from [Rap93a] © IEEE].

Angular Spread predicts correlation distances

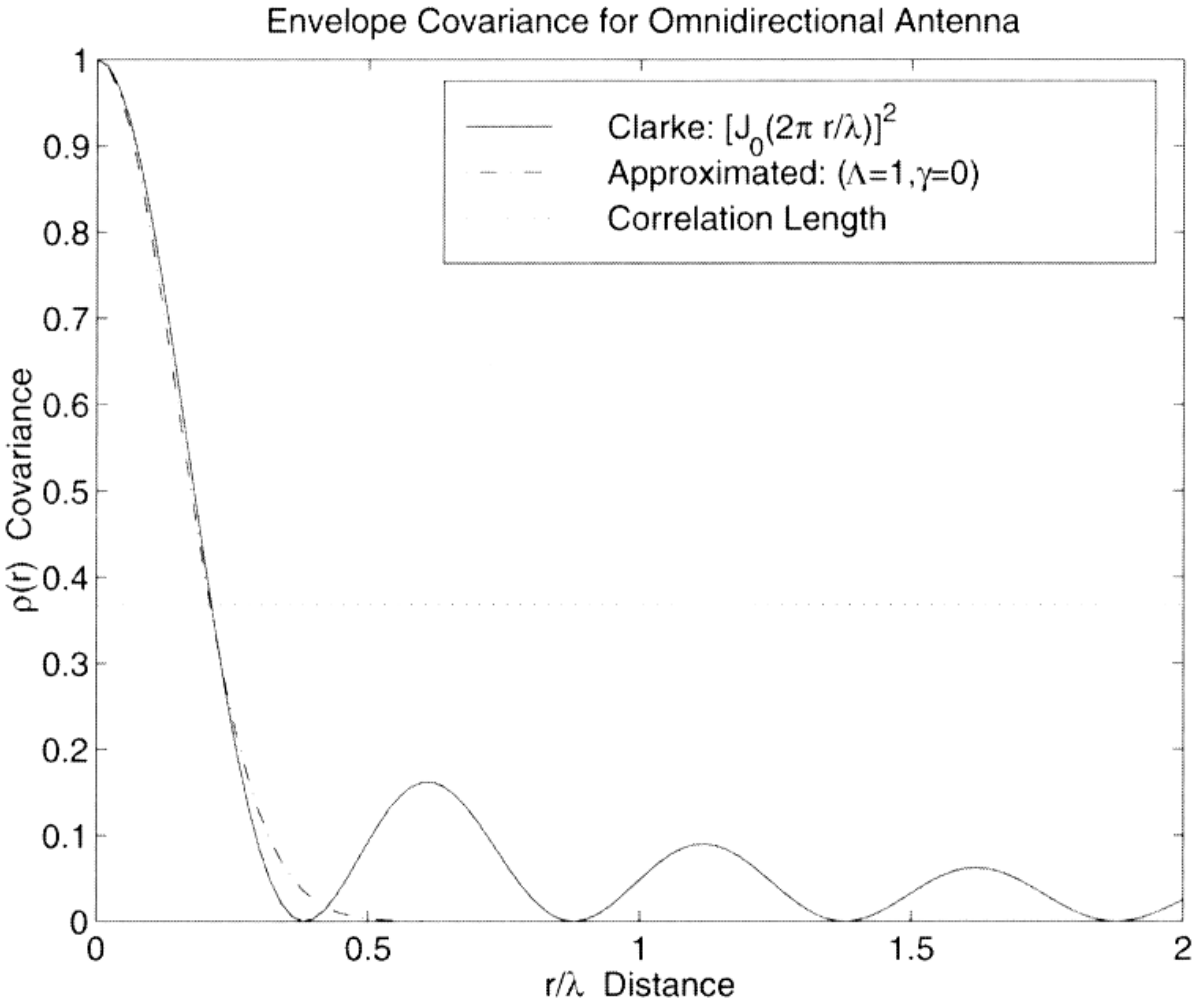

Figure 5.34 Comparison between Clarke theoretical and the shape theory approximation for envelope autocovariance functions for E_z-case [from [Dur00] ©IEEE].

Angular Spread predicts correlation distances

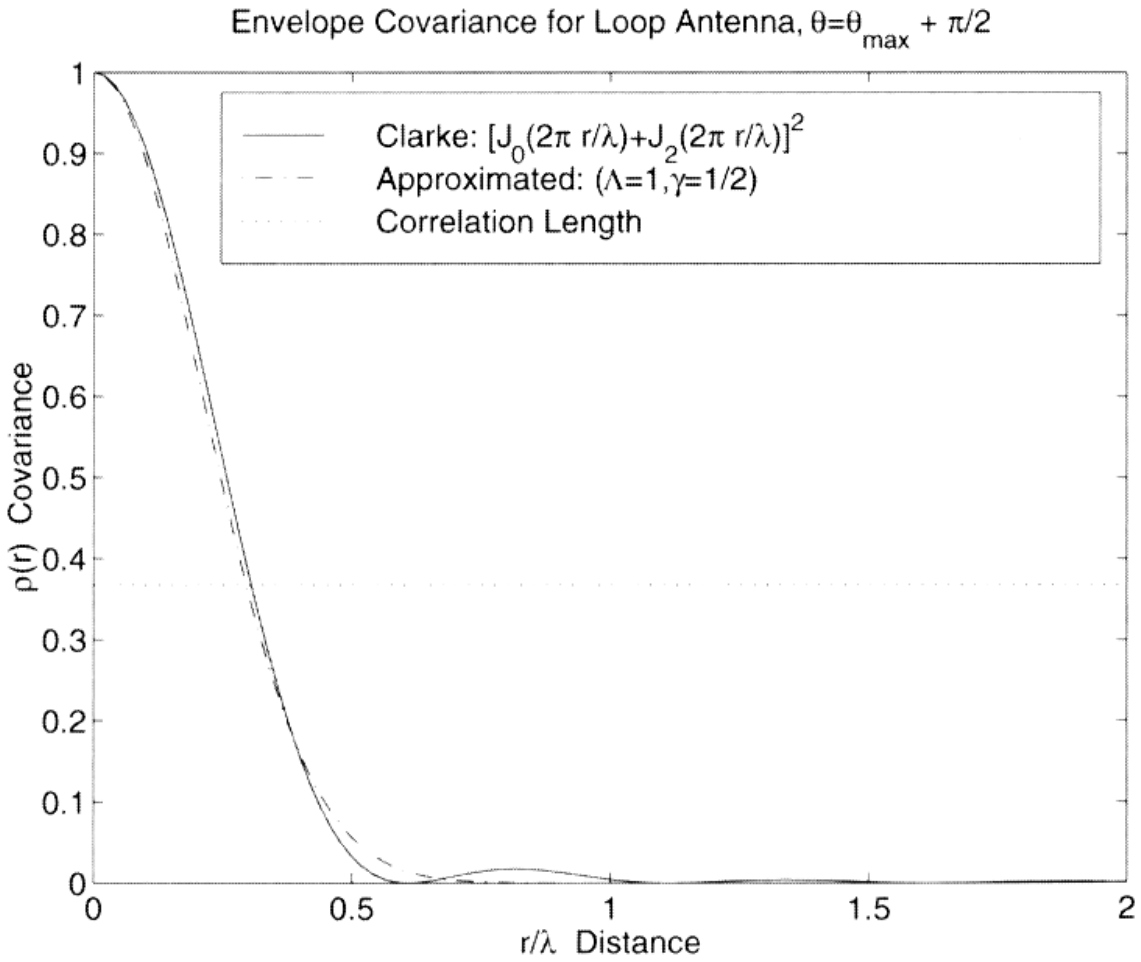

Figure 5.35 Comparison between Clarke theoretical and the shape theory approximation for envelope autocovariance functions for H_x-case [from [Dur00] ©IEEE].

Project assignment

Rayleigh fading Channel modeling:

the requirements are

- Generate a uncorrelated Rayleigh fading channel
  - Compare its histograms of the magnitude and phase responses with the theoretical PDF cures. Verify your channel modeling.
- Generate a correlated Rayleigh fading channel using
  - (a) Jake's model/modified Jake's model
  - (b) Compare the histograms of the magnitude and phase responses with the theoretical PDF cures. Verify your channel modeling.
  - (c) Verify it has the U-shape power spectrum.
  - (d) Verify that the autocorrelation is close to a zero-order Bessel function of the first kind.
- Compare the uncorrelated Rayleigh and correlated Rayleigh fading channels.

Project assignment

Multipath Rayleigh fading channel modeling

the requirements are:

- Show the power profiles of your Multipath CIRs.
- Explain the effect of the frequency selective fading (compare it with the narrowband channel by conducting and spectrum analysis.)

itance, which is the sum of depletion capacitances and the oxide capacitance is between 1 and 2×10^5 pF/cm^2. From the results obtained the total capacitance of an optimised device structure ($l_g = 1\,\mu$m, $w_g = 30\,\mu$m) is calculated to be ~ 30 fF which is small enough for applications up to 10 Gbit/s.

To test the devices a microwave setup (rise time 25 ps) was used. The devices were characterised in the triggered travelling domain mode. Single domains were triggered by gate pulses of 0·5 V and of 200 ps duration (full width at half maximum (FWHM)). The triggered current drops were 35 mA, equivalent to 55%. For the tested device the FWHM of the current drops was 260 ps which corresponds closely to the length of 30 μm between gate and anode. For shorter devices switching times of less than 100 ps could be achieved. The measured rise and fall times were 50 ps including the rise time of the experimental setup. The transconductance of the devices below the Gunn threshold was ~ 10 mS/mm which results from the large gate length ($\sim 10\,\mu$m) and from the low electron concentration of the InGaAs layer. However, optimising these parameters should lead to higher transconductances by an order of magnitude for 1 μm long gates and an improved trigger sensitivity of the devices.

Conclusion: In summary, we demonstrate for the first time the triggering of single domains in InGaAs-transferred-electron devices having a MESFET-like structure. Current drops of 35 mA with an FWHM of 260 ps were triggered by 0·5 V pulses. We tested several enhancement layers to increase the Schottky barrier height on InGaAs which is essential for the realisation of the gate electrode. Barrier heights between 0·53 and 0·67 eV were obtained. The quasi-Schottky-diodes employed as gates had reverse current densities of 10^{-3} A/cm^2 at -1 V. Further improvements in the devices can be expected by reducing the gate length and increasing the doping concentration of the InGaAs layer. From the results which were measured with actual devices (and not with large area diodes as is usually done) it can be expected that the devices can be used advantageously for high-speed applications in InP-based integrated circuits or as simple millimetre wave oscillators.

Acknowledgment: The authors would like to thank H. Newi and D. Rümmler for their contributions to the experimental work and L. Malacky for stimulating discussions. This work was financially supported by the DBP Telekom.

4th May 1993

D. Hahn, G. Zwinge and A. Schlachetzki (*Institut für Halbleitertechnik, Technical University Braunschweig, D-W-3300 Braunschweig Germany*)

References

1 KOWALSKY, W., and SCHLACHETZKI, A.: 'Analysis of the transferred-electron effect in the InGaAsP system', *Solid-State Electron.*, 1987, **30**, pp. 161–172

2 HAHN, D., HANSEN, K., and SCHLACHETZKI, A.: 'Experimental study of InGaAs transferred electron device as fast laser driver', *Electron. Lett.*, 1991, **27**, pp. 2070–2072

3 LUGLI, P., GRIMM, M., PABST, M., and LÜTH, H.: 'Travelling Gunn domains in submicron GaAs MESFETs', *Electron. Lett.*, 1991, **27**, pp. 398–400

4 DISKUS, C. G., LÜBKE, K., SPRINGER, A. L., LETTENMAYR, H. W., and THIM, H. W.:'Gunn effect in MESFET like structures', *Electron. Lett.*, 1992, **28**, pp. 980–981

5 KORDOŠ, P., MARSO, M., MEYER, R., and LÜTH, H.: 'Schottky barrier enhancement on n-$In_{0.53}Ga_{0.47}As$', *J. Appl. Phys.*, 1992, **72**, pp. 2347–2355

6 SUGETA, T., TANIMOTO, M., IKOMA, T., and YANAI, H.: 'Characteristics and applications of a Schottky-barrier-gate Gunn-effect digital device', *IEEE Trans.*, 1974, **ED-21**, pp. 504–515

7 SZE, S. M.: 'Physics of semiconductor devices' (John Wiley & Sons Inc., New York, 1981)

8 HO, M. C., HE, Y., CHIN, T. P., LIANG, B. W., and TU, C. W.: 'Enhancement of effective Schottky barrier height on *n*-type InP', *Electron. Lett.*, 1992, **28**, pp. 68–71

9 BÖTTCHER, E. H., KUHL, D., HIERONYMI, F., DRÖGE, E., WOLF, T., and BIMBERG, D.: 'Ultrafast semiinsulating InP : Fe-InGaAs : Fe-InP : Fe MSM photodetectors: Modelling and performance', *IEEE J. Quantum Electron.*, 1992, **QE-28**, pp. 2343–2357

JAKES FADING MODEL REVISITED

P. Dent, G. E. Bottomley and T. Croft

Indexing terms: Fading, Mobile radio systems

With the popular Jakes fading model, it is difficult to create multiple uncorrelated fading waveforms. In the Letter, modifications to the model are proposed which solve this problem.

Introduction: The Jakes fading model is a deterministic method for simulating time-correlated Rayleigh fading waveforms [1] and is still widely used today [2–4]. The model assumes that N equal-strength rays arrive at a moving receiver with uniformly distributed arrival angles α_n, such that ray n experiences a Doppler shift $\omega_n = \omega_M \cos(\alpha_n)$, where $\omega_M = 2\pi f v/c$ is the maximum Doppler shift, v is the vehicle speed, f is the carrier frequency, and c is the speed of light.

Using $\alpha_n = 2\pi n/N$ [1] (see Fig. 1), there is quadrantal symmetry in the magnitude of the Doppler shift, except for angles

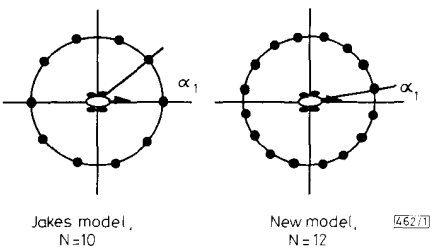

Fig. 1 *Ray arrival angles in Jakes ($N = 10$) and new models ($N = 12$)*

0 and π. As a result, the fading waveform can be modelled with $N_0 + 1$ complex oscillators, where $N_0 = (N/2 - 1)/2$. This gives

$$T(t) = K\left\{\frac{1}{\sqrt{(2)}}[\cos(\alpha) + I\sin(\alpha)]\cos(\omega_M t + \theta_0) + \sum_{n=1}^{N_0}[\cos(\beta_n) + I\sin(\beta_n)]\cos(\omega_n t + \theta_n)\right\} \quad (1)$$

where I denotes $\sqrt{(-1)}$ (j is used in Reference 1 for waveform index), K is a normalisation constant, α (not the same as α_n) and β_n are phases, and θ_n are initial phases usually set to zero. Setting $\alpha = 0$ and $\beta_n = \pi n/(N_0 + 1)$ gives zero crosscorrelation between the real and imaginary parts of $T(t)$.

To generate multiple uncorrelated waveforms, Jakes [1] suggests using phases $\theta_{n,j} = \beta_n + 2\pi(j-1)/(N_0+1)$, where $j = 1$ to N_0 is the waveform index. However, this gives almost uncorrelated waveforms j and k only when $\theta_{n,j} - \theta_{n,k} = i\pi + \pi/2$, for some integer i. Otherwise, the correlation between certain waveform pairs can be significant [5].

In this Letter, a remedy for this problem is proposed in which orthogonal functions (Walsh–Hadamard codewords) weight the oscillator values before summing. To eliminate correlation, the oscillators must have equal power. This is achieved by reformulating the Jakes model in terms of slightly different arrival angles.

Model reformulation: To provide quadrantal symmetry for *all* Doppler shifts, which leads to equal power oscillators, the following arrival angles are used (see Fig. 1): $\alpha_n = 2\pi(n - 0{\cdot}5)/N$. Following the procedure in Reference 1, this leads to the model

$$T(t) = \sqrt{\left(\frac{2}{N_0}\right)}\sum_{n=1}^{N_0}[\cos(\beta_n) + I\sin(\beta_n)]\cos(\omega_n t + \theta_n) \quad (2)$$

where $N_0 = N/4$ and the normalisation factor $\sqrt{(2/N_0)}$ gives $E\{T(t)T^*(t)\} = 1$. Moment and correlation expressions are similar to those in Reference 1, with the absence of the terms depending on α.

By using $\beta_n = \pi n/N_0$, the real and imaginary parts of $T(t)$

have equal power and are uncorrelated. Randomising θ_n provides different waveform realisations.

Multiple uncorrelated waveforms: Many application simulations require multiple uncorrelated waveforms. Waveform crosscorrelation is determined by the sum of the product of the oscillator coefficients, which can be viewed as a vector inner product. Orthogonal vectors, such as Walsh–Hadamard (WH) codewords [6], give zero inner product values with one another. Thus, with N_0 a power of two, the jth waveform can be generated using

$$T(t,j) = \sqrt{\left(\frac{2}{N_0}\right)} \sum_{n=1}^{N_0} A_j(n) \times \{[\cos(\beta_n) + I \sin(\beta_n)] \cos(\omega_n t + \theta_n)\} \quad (3)$$

where $A_j(n)$ is the jth WH code sequence in n (± 1 values). This gives N_0 uncorrelated waveforms, which can be efficiently generated by passing the original N_0 complex oscillator values through a fast Walsh transform (FWT). Correlation properties are insensitive to the random number seed used to initialise the oscillator phases θ_n.

To obtain fewer waveforms, N_w a power of two and less than N_0, groups of N_0/N_w complex oscillators can be presummed before being passed through an N_w-point FWT. It is recommended that the pre-sums draw evenly from the Doppler spectrum, e.g. $1 + 5 + 9 + 13$, $2 + 6 + 10 + 14$, etc. for $N_0 = 16$, $N_w = 4$. This corresponds to the first stages of a decimate-in-frequency form FWT. Thus, if such an FWT is used after pre-summing, the same fading waveforms will be reproduced should less pre-summing be used in another simulation run.

Numerical results: A simulation was run to generate four uncorrelated complex baseband fading waveforms using $N_0 = 16$ oscillators. With a Doppler frequency $\omega_M = 2\pi(83)$, 1 000 000 samples of each fading waveform were generated using a sampling period of 383·5 μs. For each waveform, both autocorrelation (see Fig. 2) and probability density functions agreed well with theory.

Various moments and correlation coefficient values (ρ as defined in Reference 7) are compared to theoretical values in Table 1. Complex correlation coefficients between pairs of waveforms are given in Table 2. These results indicate good model performance.

Conclusion: The Jakes fading model provides multiple time correlated fading waveforms, but the waveforms are not truly uncorrelated with one another. By reformulating the model with slightly different ray arrival angles, N_0 equal-strength oscillators result, which can then be weighted by orthogonal weighting functions, such as Walsh–Hadamard sequences, to give up to N_0 uncorrelated fading waveforms. Simulation tests confirm that the new model produces uncorrelated fading waveforms whose behaviour matches theoretical expectations.

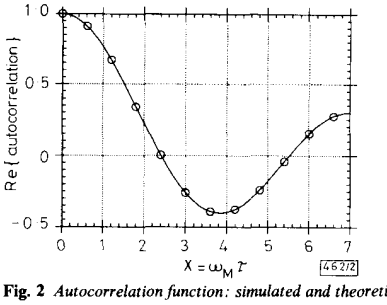

Fig. 2 *Autocorrelation function: simulated and theoretical results*
——— theory: $J_0(X)$
○ simulated

Table 2 MEASURED CORRELATION COEFFICIENTS BETWEEN WAVEFORMS

Wave (j)	Wave (k)	Crosscorrelation ($\rho\{T(t,j), T^*(t,k)\}$)
0	1	$-4{\cdot}7 \times 10^{-5} + i(2{\cdot}1 \times 10^{-5})$
0	2	$-4{\cdot}0 \times 10^{-6} + i(2{\cdot}8 \times 10^{-5})$
0	3	$-3{\cdot}2 \times 10^{-5} - i(7{\cdot}0 \times 10^{-6})$
1	2	$3{\cdot}4 \times 10^{-5} - i(4{\cdot}0 \times 10^{-6})$
1	3	$-1{\cdot}5 \times 10^{-5} - i(2{\cdot}3 \times 10^{-5})$
2	3	$2{\cdot}1 \times 10^{-5} - i(1{\cdot}0 \times 10^{-5})$

Acknowledgments: The authors would like to thank S. Chennakeshu, B. Gudmundson, and J. C. Chen for their helpful comments and suggestions.

23rd March 1993

P. Dent, G. E. Bottomley and T. Croft (*Ericsson GE Mobile Communications, Inc., 1 Triangle Drive, PO Box 13969, RTP, NC, USA*)

References

1 JAKES, W. C., JUN. (Ed.): 'Microwave mobile communications' (Wiley, New York, 1974)
2 KOILPILLAI, R. D., CHENNAKESHU, S., and TOY, R. T.: 'Low complexity equalizers for U.S. digital cellular system'. Proc. VTC '92, Denver, CO, 10th–13th May 1992
3 LO, N. W. K., FALCONER, D. D., and SHEIKH, A. U. H.: 'Adaptive equalization and diversity combining for mobile radio using interpolated channel estimates', *IEEE Trans.*, 1991, **VT-40**, (3), pp. 636–645
4 STÜBER, G. L., and YIIN, L.-B.: 'Downlink outage predictions for cellular radio systems', *IEEE Trans.*, 1991, **VT-40**, (3), pp. 521–531
5 VON ECKARDSTEIN, S., and ISAKSSON, K.: 'Kanalmodeller för radiotransmission (Channel models for radio transmission)'. Master's Thesis, Royal Institute of Technology, Stockholm, Sweden, December 1991 (in Swedish)
6 AHMED, N., and RAO, K. R.: 'Orthogonal transforms for digital signal processing' (Springer-Verlag, New York, 1975)
7 PAPOULIS, A.: 'Probability, random variables, and stochastic processes' (McGraw-Hill, New York, 1965)

WAVELENGTH-INSENSITIVE FUSED POLISHED COUPLERS

C. V. Cryan, K. P. Oakley and C. D. Hussey

Indexing terms: Optical couplers, Optical fibres

Wavelength-insensitive fused polished couplers are fabricated both from different fibres and from identical fibres where in the latter case one of the fibres is polished to such an extent that a small portion of its core is removed.

Introduction: The production of a wavelength-insensitive response in fused tapered couplers by inducing an asymmetry

Table 1 FADING PROCESS MOMENTS: SIMULATED AND THEORETICAL VALUES

Moment	Ideal	Wave 0	Wave 1	Wave 2	Wave 3
Re $\{E\{T(t,j)\}\}$	0·0	$-1{\cdot}297 \times 10^{-5}$	$-1{\cdot}446 \times 10^{-5}$	$2{\cdot}064 \times 10^{-5}$	$2{\cdot}489 \times 10^{-5}$
Im $\{E\{T(t,j)\}\}$	0·0	$-1{\cdot}030 \times 10^{-5}$	$-2{\cdot}0 \times 10^{-7}$	$-8{\cdot}39 \times 10^{-6}$	$-5{\cdot}36 \times 10^{-6}$
$E\{\text{Re}\{T(t,j)\}^2\}$	0·5	0·499827	0·499710	0·499772	0·499813
$E\{\text{Im}\{T(t,j)\}^2\}$	0·5	0·499825	0·499722	0·499755	0·499770
$\rho\{\text{Re}\{T(t,j)\}, \text{Im}\{T(t,j)\}\}$	0·0	$5{\cdot}793 \times 10^{-5}$	$-9{\cdot}206 \times 10^{-5}$	$-8{\cdot}38 \times 10^{-6}$	$-1{\cdot}056 \times 10^{-5}$
Re $\{E\{T(t,j), T^*(t,j)\}\}$	1·0	0·999985	0·999807	0·999880	0·999907

Modified Jakes' Model for Simulating Multiple Uncorrelated Fading Waveforms

Yingbo Li & Y.L. Guan

School of EEE
Nanyang Technological University
Nanyang Avenue, Singapore 639798
Tel: +65-790 5875
Fax: +65-793 3318
E-mail: p140542430@ntu.edu.sg

Abstract - Two ways for modifying the classical Jakes' fading simulator to generate multiple uncorrelated fading waveforms are proposed. The 1st and 2nd order statistics of individual output waveforms are shown to agree well with theoretical expectations. The cross correlation between different waveforms is nearly zero. These fading simulators are expected to be useful in the investigations of frequency-selective and diversity-combined multipath fading channels.

I. Introduction

The Jakes' deterministic fading model is an established method for simulating time-correlated Rayleigh flat fading waveforms. For simulation of frequency selective and diversity combined fading channels, it is desirable to extend the Jakes' model to produce multiple uncorrelated fading waveforms. This has been done in [1], in which the authors reformulate the Jakes' Model with slightly different arrival angles of the incident multipath rays and apply orthogonal weighting functions (Walsh-Hadamard codewords) on the oscillators in the model to produce uncorrelated outputs. In this paper, two other forms of modified Jakes' model, with simpler structures that do not require the use of orthogonal weighting functions, are proposed. The technique used here is to generate independent fading signals by using the same set of sinusoidal generators as in [1,2] but with a suitable set of phase shifts on each of them. The 1st and 2nd order statistics of the output waveforms are verified against theoretical expectations. In this paper, the model structure, its derivation and verification are presented. Its advantage over other forms of fading simulator (eg. filtered Gaussian Noise model) lies in its greatly reduced executing time and capability for simultaneous generation of multiple uncorrelated fading signals.

II. Simulator Structures

Following [1,2], our simulator essentially models the fading signal as a discrete sum of in-phase & quadrature-phase sinusoidal signals with different Doppler frequencies and appropriate phase shifts.

Model I

For this model, we adopt symmetrical values for the Doppler shift components (ω_n) and initial phase shift (θ_{nj}) as in [1]. The in-phase and quadrature-phase components of the j^{th} path fading waveform are, respectively:

$$X_{cj}(t) = 2\sum_{n=1}^{No} \cos\theta_{nj}\cos(\omega_n t+\pi j/2) \qquad (1)$$

$$X_{sj}(t) = 2\sum_{n=1}^{No} \sin\theta_{nj}\cos(\omega_n t+\pi j/2) \qquad (2)$$

where $\theta_{nj} = \frac{\pi n j}{N_0}$, (j=1, 2,..., N_0-1);

$\omega_m = 2\pi V/\lambda$; V = vehicle speed;

λ = carrier wavelength;

$\omega_n = \omega_m \cos\frac{2\pi(n-0.5)}{N}$;

$N = 4(N_o+1)$; N_0 = number of oscillators.

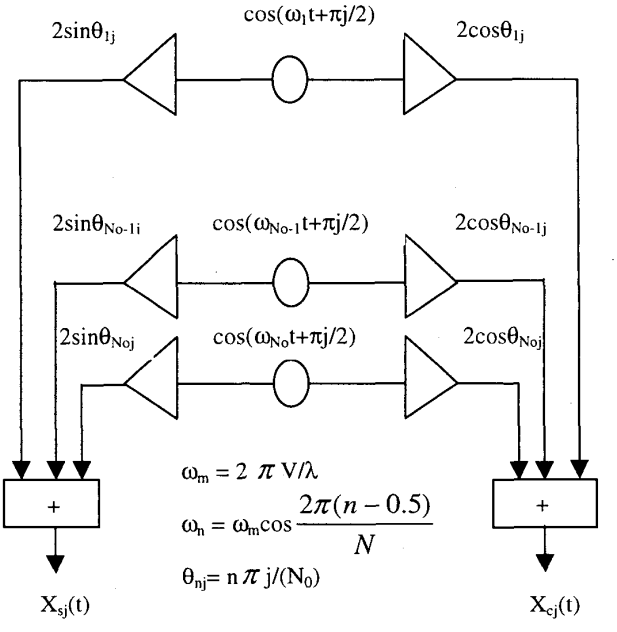

Fig.1. Model I structure (the j^{th} path)

0-7803-5718-3/00/$10.00 ©2000 IEEE.

The selection for θ_{nj} is to ensure that the in-phase and quadrature-phase components have equal average power and are uncorrelated. The additional phase $\pi j/2$ is imposed to cancel out the cross correlation among quadrature components of different paths. The choice of N is to give same number of oscillators (N_0) as the classical Jakes' model [2]. Figure 1 depicts the structure for the j^{th} path of this model:

Model II

This model uses the same set of oscillators as suggested by Jakes [2] but with adjusted initial phase shifts, θ_{nj} & α, The I & Q components of j^{th} path signal are:

$$X_{cj}(t) = 2\sum_{n=1}^{No}\cos\theta_{nj}\cos(\omega_n t+\pi j/2) + 2|\cos\alpha|\cos(\omega_m t+\pi j/2) \quad (3)$$

$$X_{sj}(t) = 2\sum_{n=1}^{No}\sin\theta_{nj}\cos(\omega_n t+\pi j/2) + 2\sin\alpha\cos(\omega_m t+\pi j/2) \quad (4)$$

where, $\alpha=\pi j$; $\theta_{nj} = \dfrac{\pi n j}{No+1}$, j=1, 2,..., N_o;

$\omega_m = 2\pi V/\lambda$; $\omega_n = \omega_m\cos\dfrac{2\pi n}{N}$; $N = 4N_o+2$.

$|\cos\alpha|$ takes positive value of $\cos\alpha$.

The design of parameters follows similar rules as in Model I.

III. Derivation of Simulation Parameters

In order to generate multiple uncorrelated Rayleigh fading signals, the following conditions must be ensured:

a. $\overline{X_{cj}^2} = \overline{X_{sj}^2}$ (5)

b. $\overline{X_{cj} * X_{sj}} = 0$ (6)

c. $\overline{T_i \times T_j} = \overline{T_i} \times \overline{T_j}$ (7)

(or $\overline{X_{ci} \times X_{cj}} = 0; \overline{X_{si} \times X_{sj}} = 0$)

where,

$$\overline{X_{cj}^2} = N_0 + \sum_{n=1}^{No}\cos 2\theta_{nj} \quad (8a)$$

$$\overline{X_{sj}^2} = N_0 - \sum_{n=1}^{No}\cos 2\theta_{nj} \quad (8b)$$

$$\overline{X_{cj} \times X_{sj}} = \sum_{n=1}^{No}\sin 2\theta_{nj} \quad (8c)$$

$$\overline{X_{ci} \times X_{cj}} = \sum_{n=1}^{No}[(\cos(\theta_{ni}+\theta_{nj}) + \cos(\theta_{ni}-\theta_{nj}))\times \cos((i-j)\pi/2)] \quad (8d)$$

$$\overline{X_{si} \times X_{sj}} = \sum_{n=1}^{No}[(\cos(\theta_{ni}+\theta_{nj}) - \cos(\theta_{ni}-\theta_{nj}))\times \cos((i-j)\pi/2)] \quad (8e)$$

$$\overline{X_{ci} \times X_{sj}} = \sum_{n=1}^{No}[(\sin(\theta_{ni}+\theta_{nj}) + \sin(\theta_{ni}-\theta_{nj}))\times \cos((i-j)\pi/2)] \quad (8f)$$

The above expressions dictate the selection of parameters shown earlier for two models. The selection is, however, not unique. Those shown earlier are only one possible set of selection.

IV. Verification

For verification purpose, the proposed models are simulated with the following settings: $\omega_m=2\pi\times100$Hz, $N_o=16$, sample size=1,000,000, sampling period=10^{-5} s. The probability density functions (PDFs) and autocorrelation functions of output waveforms are given in Fig. 2 to Fig. 5.

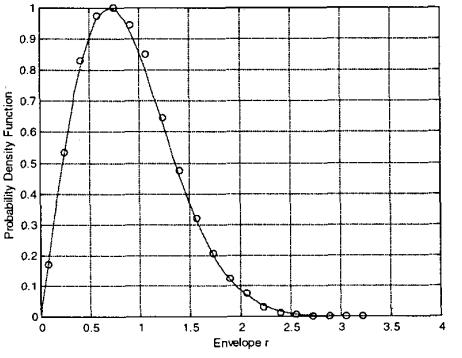

Fig. 2. typical PDF of Model-I output waveforms
—— theory: Rayleigh
o simulated

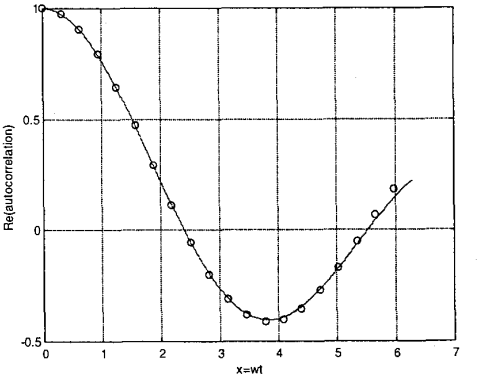

Fig. 3. typical autocorrelation of Model-I output waveforms
—— theory: $J_o(x)$ w: doppler ω
o simulated t: time delay

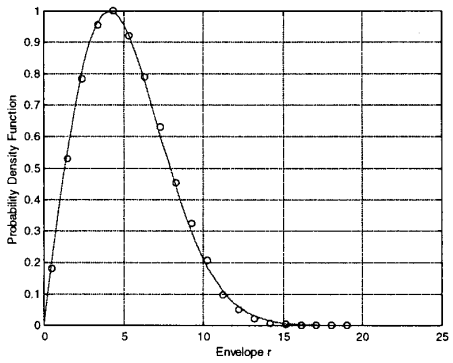

Fig. 4. typical PDF of Model-II output waveforms

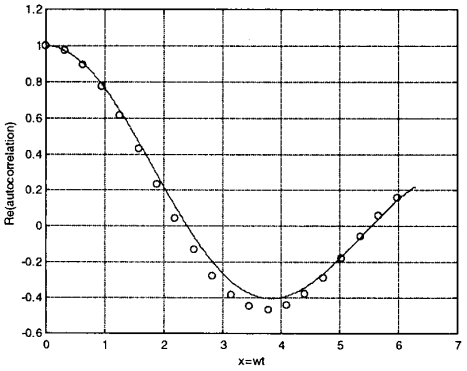

Fig. 5. typical autocorrelation of Model-II output waveforms

On the other hand, the cross-correlation coefficients between the I&Q quadrature components of the output waveforms are observed to be less than ±0.01, while the cross-correlation coefficients between the envelopes of output waveforms are observed to be less than ±0.1.

Table I: cross correlation coefficients between the envelopes of model-I output waveforms

x-corrcoef.	Path1	Path2	Path3	Path4	Path5	Path6	Path7	Path8
Path1	1	-0.016	-0.1	-0.05	-0.096	-0.038	-0.1	-0.036
Path2		1	-0.013	-0.098	-0.02	-0.1	-0.02	-0.1
Path3			1	-0.009	-0.087	-0.014	-0.1	-0.05
Path4				1	-0.015	-0.096	-0.03	-0.095
Path5					1	-0.025	-0.1	-0.04
Path6						1	-0.034	-0.1
Path7							1	-0.027
Path8								1

Table II: cross correlation coefficients between quadrature (In phase) components of model-I output waveforms

x-corrcoef.	Path1	Path2	Path3	Path4	Path5	Path6	Path7	Path8
Path1	1	-0.007	0.002	0.006	-0.001	-0.004	-0.000	0.004
Path2		1	-0.007	0.0003	0.006	-0.000	-0.005	-0.000
Path3			1	-0.007	-0.000	0.006	-0.000	-0.003
Path4				1	-0.007	-0.000	0.004	-0.000
Path5					1	-0.006	-0.000	0.003
Path6						1	-0.005	-0.000
Path7							1	-0.004
Path8								1

Table III: cross correlation coefficients between the envelopes of model-II output waveforms

x-corrcoef.	Path1	Path2	Path3	Path4	Path5	Path6	Path7	Path8
Path1	1	-0.05	-0.09	-0.04	-0.08	-0.025	-0.09	-0.013
Path2		1	-0.046	-0.09	-0.037	-0.09	-0.01	-0.09
Path3			1	-0.03	-0.09	-0.02	-0.097	-0.09
Path4				1	-0.027	-0.08	-0.034	-0.095
Path5					1	-0.02	-0.08	-0.04
Path6						1	-0.014	-0.09
Path7							1	-0.027
Path8								1

Table IV: cross correlation coefficients between quadrature (In phase) components of model-II output waveforms

x-corrcoef.	Path1	Path2	Path3	Path4	Path5	Path6	Path7	Path8
Path1	1	-0.007	0.0016	0.0076	-0.002	-0.008	0.0015	0.0095
Path2		1	-0.006	0.0011	0.0083	-0.002	-0.008	-0.000
Path3			1	-0.006	0.0009	0.0075	-0.000	-0.008
Path4				1	-0.006	-0.000	0.0076	-0.000
Path5					1	-0.006	0.0008	0.007
Path6						1	-0.005	0.0001
Path7							1	-0.005
Path8								1

V. Conclusion

The classical Jakes' model has been reformulated by introducing different arrival ray angles for Doppler shift components (ω_n) and additional phase shift to every oscillator in the simulator model to generate multiple uncorrelated fading waveforms. The PDF, autocorrelation characteristics of the simulated waveforms are demonstrated to agree closely with theory. The cross-correlation characteristics among all waveforms are found to be nearly zero. These new models are easy to construct and efficient to run compared to fading simulator using filtered Gaussian Noise approach.

REFERENCE

[1] Dent,P; Bottomley,G.E.; Croft, T. "Jakes Fading Model Revisited", *Electronics Letters*, Vol.29, No.13, 24 June 1993, pp.1162-1163.

[2] Jakes, William C. *Microwave Mobile Communications*. New York, Wiley, 1974.